CHALMERS
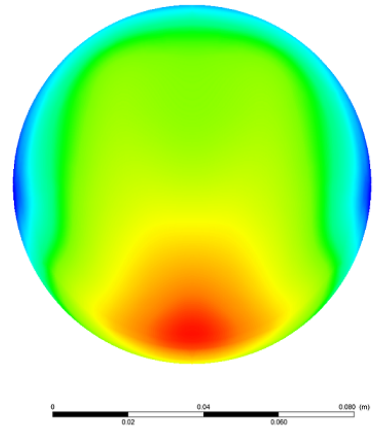

FLOW MALDISTRIBUTION IN EXHAUST AFTERTREATMENT SYSTEMS - NUMERICAL SIMULATIONS

PRATHEEBA CHANDA NAGARAJAN

THESIS FOR THE DEGREE OF LICENTIATE OF ENGINEERING IN THERMO AND FLUID DYNAMICS

FLOW MALDISTRIBUTION IN EXHAUST AFTERTREATMENT SYSTEMS - NUMERICAL SIMULATIONS

PRATHEEBA CHANDA NAGARAJAN

Department of Mechanics and Maritime Sciences
CHALMERS UNIVERSITY OF TECHNOLOGY

Göteborg, Sweden 2022

FLOW MALDISTRIBUTION IN EXHAUST AFTERTREATMENT SYSTEMS - NUMERICAL SIMULATIONS
PRATHEEBA CHANDA NAGARAJAN

Cover Picture: Illustration of length scales involved in a diesel oxidation catalyst.

ABSTRACT

To comply with the stringent emission norms under every driving condition, including the coldstart conditions and Real Driving Emissions (RDE) tests, accurate models that capture the spatial and temporal variation of flow distribution information in Exhaust AfterTreatment Systems (EATS) are required. This study is aimed at characterizing and quantifying flow distribution in EATS under transient conditions with realistic geometry that illustrates the complex nature of the flow conditions. Catalytic converters are employed to control emissions. Space limitation in the exhaust line creates non-uniform flow in terms of flow through bends and dead volumes. This limits the performance of the EATS. The flow from the engine does not proceed uniformly to the EATS, creating flow maldistribution at the inlet of EATS. Due to the non-uniform flow, the velocity, temperature and concentrations at the exit are functions of the flow distribution at the inlet. Reactor models that predict conversion of emissions require this information for accurate prediction of conversion of emission gases at the tail pipe.

To this end, transient Computational Fluid Dynamics (CFD) simulations are performed to understand the evolution of the flow profiles in the catalytic converter, both under non-reactive and reactive conditions. The flow from the engine is turbulent. Hence, Unsteady Reynolds Averaged Navier Stokes (URANS) equation is used solve for the transport equations to obtain the profiles of velocity, temperature and concentration in the catalytic converter. The turbulence closure is achieved by using $\kappa - \omega$ model . The catalyst is modeled as porous media.

This thesis presents the results of both non-reactive and reactive simulations, to illustrate the importance of flow and temperature non-uniformity and pulsations respectively. Flow uniformity index is used to characterize the extent of variation of the flow parameters in any catalyst plane. In addition to the uniformity index, contours and histograms are employed to demonstrate the non-uniform flow field. The specification of inlet fluctuations is also required to emulate real time flow to a catalytic converter.

The contours of velocity and histograms show that there is significant distribution of the flow variables at the catalyst outlet. This illustrates that a single channel model is very ideal, and it requires flow distribution information to predict tail pipe concentrations accurately. The inclusion of flow distribution information in EATS model can make the model more accurate. These models can be then used in control and monitoring of emissions from automobiles. This will take a step closer towards Zero Emissions.

Keywords: Exhaust AfterTreatment Systems, CFD Simulations, Flow maldistribution, Transient, Uniformity Index, Catalyst, Reactive flows

Acknowledgements

siblings Savithri and Shrenivas have held me up in my most difficult times. I thank Harini and Achyuth for sharing their love. Thank You Santhosh, Vasudha and Guruprasad, for the affection and care you shower on me. I thank my uncles and aunts for their affection for me.

Pratheeba

Gothenburg
June 2022.

To
My Family and My Advisors
Thank you for showing me that hope is the best of good things!

Contents

List of Figures

List of Tables

Nomenclature

Abbreviations

3D	**3 D**imensional
ASC	**A**mmonia **S**lip Catalyst
CARB	**C**alifornia **A**ir **R**esources **B**oard
CDR	**C**onvection **D**iffusion **R**eaction
CI	**C**ompression **I**gnition
COPD	**C**ompulsory **O**bstructive **P**ulmonary **D**isorder
CPSI	**C**ells **P**er **S**quare **I**nch
DES	**D**etached **E**ddy **Simulation**
DOC	**D**iesel **O**xidation **C**atalyst
DPF	**D**iesel **P**articulate **F**ilter
EATS	**E**xhaust **A**fter**T**reatment **S**ystems
EEA	**E**uropean **E**nergy **A**gency
EGR	**E**xhaust **G**as **R**ecirculation
EU	**E**uropean **U**nion
GHSV	**G**as **H**ourly **S**pace **V**elocity
GPF	**G**asoline **P**articulate **F**ilter
HC	**H**ydro**C**arbons
ICE	**I**nternal **C**ombustion **E**ngines
LNT	**L**ean **N**Ox **T**rap
MFC	**M**ass **F**low**C**ontrollers
MUSCL	**M**onotonic **U**pstream-centered **S**cheme for **C**onservation **L**aws
OSC	**O**xygen **S**torage **C**atalyst
PEMS	**P**ortable **E**mission **M**easurement **S**ystems
PIV	**P**article **I**mage **V**elocimetry
PM	**P**articulate **M**atter
POCS	**P**eriodic **O**pen **C**ellular **S**ubstrates
RDE	**R**eal **D**riving **E**missions
SCM	**S**ingle **C**hannel **M**odel
SCR	**S**elective **C**atalytic **R**eduction
SI	**S**park **I**gnition
SIMPLE	**S**emi **I**mplicit **P**ressure **L**inked **E**quation

SST	**S**hear **S**tress**T**ransport
TWC	**T**hree **W**ay **C**atalytic Converter
UHC	**U**nburned **H**ydro**C**arbons
UI	**U**niformity **I**ndex
URANS	**U**nsteady **R**eynolds **A**veraged **N**avier- **S**tokes

Chemical Species

CO_2	Carbon dioxide
CO	Carbon monoxide
H_2	Hydrogen
N_2	Nitrogen
NO_2	Nitrogen dioxide
NO_x	Nitrogen oxides
NO	Nitric oxide
O_2	Oxygen
SO_x	Sulphur oxides

Greek Letters

α	permeability of fluid in porous media model
β	Closure constant
β^*	Closure constant
δ_{ij}	Kronecker delta
γ	Ratio of β and β^*
γ_a	Flow uniformity index
λ	Thermal conductivity of fluid
μ	Molecular viscosity
μ_t	Turbulent viscosity
∇	Gradient operator
ν_t	Turbulent kinematic viscosity
ω	Specific dissipation rate
$\overrightarrow{v}$	phase velocity in porous media
Φ	Dissipation function
ϕ	Constant in k-ω model
ϕ_1	Inner constant 1
ϕ_2	Inner constant 2
ϕ_a	Area weighted average of flow variable

ϕ_i	flow variable at face i
ρ	Fluid density
σ_ω	Turbulent Prandtl number for specific dissipation rate ω
σ_k	Turbulent Prandtl number for turbulent kinetic energy k
$\sigma_{\omega 2}$	Closure constant
τ_{ij}	Reynolds stress tensor
ε	Turbulent dissipation rate
S_{ij}	Mean Strain rate tensor

English Symbols

$u_i',\ u_j'$	Fluctuating velocity in tensor notation
$\bar{P}$	Mean pressure
$\bar{q}_i$	Mean heat flux
$\bar{T}$	mean temperature
$\bar{u}_i,\ \bar{u}_i$	Mean velocity in tensor notation
$\bar{J}_i$	Mean species flux due to diffusion
$\bar{Y}$	Mean species mass fraction
Ω	Vorticity magnitude
A	Arrhenius frequency factor
A_i	Face area
C_p	Specific heat capacity of fluid
C_{ij}	Coefficient of inertial resistance of porous media
D_{ij}	Coefficient of viscous resistance of porous media
E_A	Activation energy
F_1	Damping function
F_2	Damping function
I	Turbulent intensity
k	Turbulent kinetic energy
P	Production limiter
R	Source term for reaction rate
R_{gas}	Universal gas constant
S	Specific area of a catalyst
S_i	Source term
t	time
T'	Fluctuating temperature
x_j	Position vector in tensor notation
d	Distance from the field point to the nearest wall

1   Introduction

This chapter provides a brief outline of emissions from the automobiles, the need for the 'aftertreatment', and the operational features of exhaust aftertreatment systems (EATS). The objectives of the thesis conclude the introduction section.

1.1   Emissions from automobiles and their effects

The role of transportation in global economy is significant. This is reflected in the increase in the number of automobiles plying on the roads. Road transport is also a significant contributor to emissions, and is a cause for climate change, both on short and long terms. Nearly 72 % of the greenhouse gas emissions are from road transport [1]. Figure 1.1 shows the percentages of greenhouse gas emissions by different sectors in the transportation industry and the split of share of different modes in the road transport [1]. This number since 2017, would have increased until now, owing to the increase of number of vehicles. Internal Combustion engines (ICE) were popular until recent times, for their compact and robust nature, and the range and applicability that they offer. Despite of many advantages, the emissions from IC engines are a cause of serious concern. Carbon monoxide, oxides of nitrogen, unburned hydrocarbons, soot and particulate matter (PM) are the emissions along with carbon dioxide. Carbon compounds in the engine-out emissions arise due to insufficient oxygen concentration and imperfect mixing within the cylinder. Air that is supplied as oxidiser and the high in-cylinder temperatures are the main reasons for oxides of nitrogen in the engine-out exhaust [2]. Clean fuel has contributed to near-zero sulphur containing gases in the exhaust and reduction of 35% of PM in the European Union (EU) since 2000 [3].
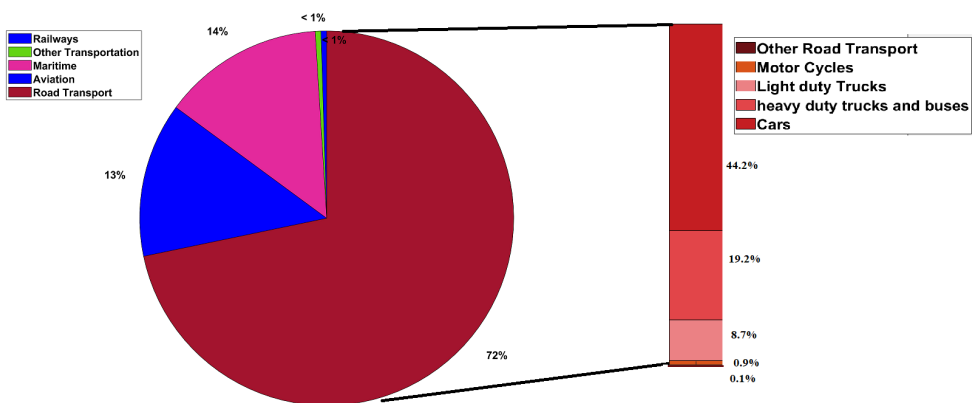
Figure 1.1: *GreenHouse Gases Emissions by Sources from the transportation sector - data from 2017. (Source: European Environment Agency EEA) [1]*

1.2 Composition of engine exhausts

The combustion of hydrocarbon based fuels or other fuel (H_2) with air in the Internal Combustion Engines (ICE) can be complete or incomplete. CO is the product of incomplete combustion, whereas CO_2 is formed under complete combustion conditions. The bulky fuel molecule also produces small but significant amounts of smaller hydrocarbons and PM. The composition of typical diesel engine exhaust and gasoline engine exhaust are given in Table 1.1 [4]. The emissions depend on the the air-fuel ratio. The engine-out emissions require to be converted to CO_2 and water. Oxides of nitrogen that are created in the combustion process have to be reduced to N_2. To achieve these reactions, catalytic converters are used [5]. Other possible options to reduce emissions are by modification of the engine design, use of Exhaust Gas Recirculation (EGR) and use of alternate fuels and lubricating oils [6].

Table 1.1: Emissions from Diesel and Petrol Engines [4].

Mode	Range of Component		Units
	Diesel	petrol	
CO_2	7	10	%
CO	$10-15$	0.5	%
H_2O	$1.4-7$	10	%
CO	$300-1200$	5000	ppm
NO_x	$350-1000$	900	ppm
HC	$50-330$	350	ppm
H_2	$100-400$	1700	ppm
SO_x	$10-100$		ppm
PM	65		mg/m^3
N_2	Remaining	Remaining	%

Automotive emissions are detrimental to living organisms, in particular to human life. They also impact the ecosystem by affecting the ambient air quality and influence climate change [7]. The health effects due to short term exposure are Chronic Obstructive Pulmonary Disease (COPD), respiratory ailments like wheezing, asthma, cough, allergic reactions. The long term exposure lead to chronic asthma, cardio vascular diseases, increase in rates of abortion [8]. About 2g of carbon monoxide is emitted per km run by a car [2]. CO has a much larger affinity to haemoglobin (approximately 240 times than oxygen), it binds to haemoglobin, and thereby reduces the oxygen carrying capacity of the blood, leading to hypoxic condition [9]. Oxides of nitrogen cause inflammation in the respiratory organs. These gases also participate in the formation of ozone at the ground level. Ozone affects the respiratory muscles, constricting and trapping air in the alveoli. Exposure to Particulate emissions are likely to cause irritation along the respiratory tract, shortness of breath, coughing and sneezing. Chronic effects of PM include asthma and cardio vascular diseases [10]. Unburnt hydrocarbons are carcinogenic and they react with NO_2 to form ground level ozone. The ground level ozone is an irritant and mutagenic

agent.

1.3 Legislations
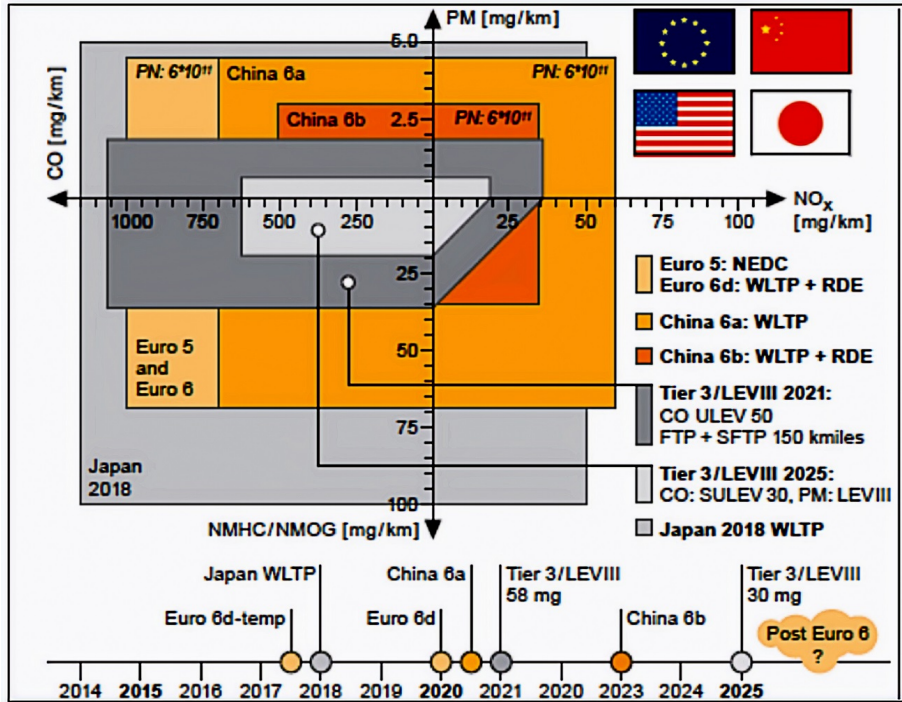
Figure 1.2: *Emission Legislations from 2012 - 2025 and Phase-In Timing in different countries. (Source:Continental Automotive) [11]*

The effects of pollution on ambient air quality was recognized as early as 1943. During the summer of 1943, the amount of air pollutants in California was so severe that the visibility was only three blocks [12]. The population of Los Angeles complained about burning of eyes and the respiratory tract and nausea. It was thought that there was a gas attack and the cause was thought to be a butadiene plant that operated in the vicinity. Efforts were taken to shut down the plant. The smog, though did not abate. A first air pollution control body named Los Angeles County air pollution control board was formed. This regulatory body standardized and monitored the operations of plants that contributed to air pollution - power plants and oil refineries. In the early 1950s, Dr Arie Haagen - Smit discovered that the main reasons for the smog were the automobile emissions. Following this discovery, in 1966, tail pipe emissions regulations were formulated in California. The California Air Resources Board (CARB) was established in 1966. The CARB since then, has been a pioneer in setting emissions standards. This led to the development of various

catalytic converters. After CARB, other states in the United States and other countries have been implementing emission control legislations .

1.4 Euro legislation norms

Similar to the CARB, the European Union (EU) had also devised emission norms. The first norm named Euro 1 was implemented in 1992. Since then, the norms are becoming increasingly stringent and tight. The EU norms comparing the amounts of CO, PM and NO_x are shown in figure 1.3. The size of the bubble is proportional to the emissions level. The ordinate is the gram of pollutant per km run of the vehicle and the abscissa is the year of EU norm. The Euro VI (d) puts a cap on PM and NO_x to near zero levels per km run of the vehicle. There are also performance checks at various driving conditions like urban, rural zones etc. Similar norms exist for heavy duty vehicles too, the difference between the light duty standards and the heavy duty standards is that the former is expressed as g per km run by the vehicle, whereas the latter is expressed as g per kWh [13].
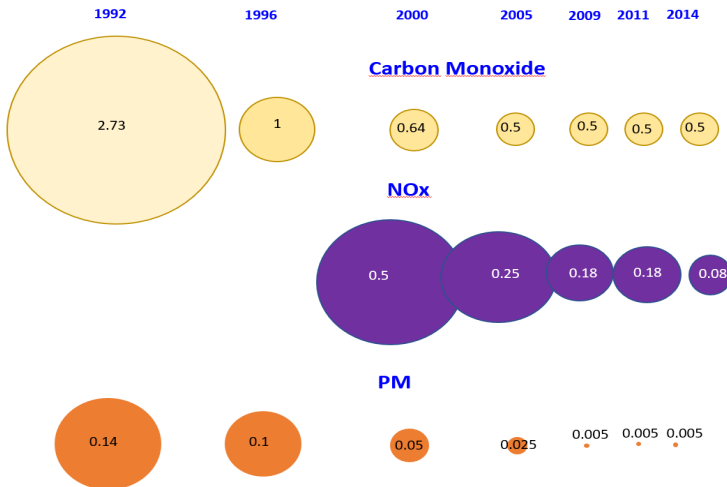
Figure 1.3: *Euro Emission Standard levels between 1992 and 2022 for diesel light duty vehicles in grams per km run (Bubbles not to scale)*

1.5 Driving conditions

A vehicle can be driven under carefully controlled laboratory environment, for example, on a chassis dynamometer, or on road. The emissions are then measured using portal emission measurement systems (PEMS) [14]. Three driving conditions are important from an emissions point of view. First of them, the coldstart driving, is the case when

the vehicle is started from rest. During coldstart, emissions are highest, as the catalyst is yet to light-off. The engine exhaust warms up the EATS as it runs, the time required depends on the thermal inertia. Second important RDE covers a wide variety of driving conditions and measuring the associated emissions using PEMS. This procedure depends on the driving cycle adopted and is carried out to bring down the gap between 'Laboratory Condition Emissions' and Actual On-road driving condition emissions. Under Euro VI(d), the vehicle has to comply emission legislations under cold start and RDE [15].

1.6   Exhaust AfterTreatment Systems

To be able to comply with the legislation norms, the engine out emissions need to be treated. This is done by using catalytic reactions, as the potential barrier for a catalysed reaction is much smaller than its uncatalysed counter part. One or more of catalytic devices are used to treat the engine-out emissions, often referred to as the exhaust treatment train. To suit the nature of diesel exhaust that is rich in NOx and PM, the aftertreatment train consists of one or more of the following: Diesel Oxidation Catalyst (DOC), Diesel Particulate Filter (DPF), Selective Catalytic Reduction (SCR) unit, Ammonia Slip Catalyst (ASC) and Lean NO_x Trap (LNT). The sequence of exhaust aftertreatment systems for a petrol engine would be either a Three-Way Catalytic converter (TWC), Gasoline Particulate Filter (GPF), oxidation catalyst and NOx adsorber catalysts [16].

DOC's are employed to oxidize unburned hydrocarbons and carbon monoxide.Some of the PM are also oxidized. DOC's are placed right after the engine and before the SCR unit to facilitate oxidation of NO to NO_2. SCR of NO_2 is faster than NO reduction. DPF is used to trap particulates. SCR is used to reduce oxides of nitrogen to atmospheric nitrogen by using a reducing agent. The reducing agent is usually ammonia, obtained by hydrolysis of urea. In order to have complete conversion, ammonia dosage is increased, this in turn leads to ammonia slip to the atmosphere. ASC is placed after the SCR to minimize ammonia slip. Hydrocarbons can also be used as reducing agents. TWC is widely used in stoichiometric SI engines, and this reduces NO to N_2 and oxidises CO and HC to CO_2 and water vapor. Oxidation catalyst oxidises CO and HC. The particulate emissions reduction is achieved by GPF.

1.7   Objectives

This project involves understanding flow distribution in automotive catalytic converters. Understanding flow distribution is imperative, as knowledge of flow, temperature and concentration profiles help in optimizing the converters and reducing emissions. The flow and temperature distribution behavior is also important during cold start and under RDE conditions. By incorporating the flow distribution data, a reactor model to predict the conversion at the catalyst outlet will become more accurate. The approach of this work includes both experiments and simulations. The main objective is to obtain the information about the representative channel(s) in the monolith.

The objectives of this work are:

- To perform relevant transient experiments to capture temperature at the inlet and outlet of the catalyst, by employing thermocouples for measurements.

- To obtain experimental data that will help to tune the model parameters, viz., heat transfer coefficients.

- To perform reactive and non-reactive simulations and to quantify flow maldistribution in terms of uniformity index.

- To evaluate the effect of inlet pulsations and fluctuations on the time-averaged conversion at the catalyst inlet through reactive simulations.

1.8   Organization of the thesis

The thesis is organized as follows: Chapter 2 introduces the background, the necessary theory for understanding flow maldistribution and the factors that affect flow distribution and the literature available for understanding flow maldistribution. The experimental details of the project are presented in Chapter 3. Chapter 4 describes the Computational Fluid Dynamics (CFD) modeling and simulation. The relevant boundary conditions and the other model details like the porous media approximation are discussed. Chapter 5 discussed the results and discusses the implications of the results. The conclusion of the work and further outlook are presented in Chapter 6. The contribution of this thesis to the flow distribution literature is presented in Chapter 7.

2 Background

The theoretical aspects of catalytic converter, with equations of change are explained in this chapter. Construction details and salient features of the experimental rig are also discussed in this chapter. The theory of flow maldistribution is also presented here.

2.1 Historical note on catalytic converters

The emissions from compression ignition (CI) engines are loaded with NO_x due to high in-cylinder temperatures whereas spark ignited (SI) engines emissions have carbon monoxide CO and unburned hydrocarbons (UHC) along with CO_2. These emissions have to be treated before they exit in the tail pipe, in order to be well within the legislation limits. This can be achieved by using catalytic converters. The catalytic converters were first envisaged by Eugene Houdry (1892-1962). The invention of three-way catalytic converter (TWC) and oxygen storage catalysts (OSC) are attributed to Dr Haren S Gandhi (1941 - 2010).

Petroleum refining yields fractions that are used as fuel for automotive vehicles. Eugene Houdry is a name familiar with catalytic cracking. He used heavy tar fractions to produce gasoline like motor fuels. He worked with companies that wanted to improve Octane number, without resorting to leaded petrol. The fixed bed catalytic converter that converted the heavy tar was experiencing high coke depositing and thereby poisoning catalysts. The plant had to be shutdown every time, until the coke was burnt and the catalyst was regenerated. Warren Lewis (of the Lewis number, which is the ratio of momentum thermal diffusivity to mass diffusivity) and Edwin Gilliland (of the Fenske-Underwood-Gilliland equation for rigorous design of multicomponent distillation) were recruited as consulting engineers to solve this issue. They modified the fixed bed unit to a moving bed catalytic cracking unit and created possibility of regeneration without the need to shut down and restart the catalytic cracking unit.

Eugene Houdry went on to develop the first-ever catalytic converter for treating smoke-like emissions from vehicles as early as 1950s. Los Angeles was engulfed in smog and the ambient air quality was deteriorated. Houdry identified that the exhaust gases from the cars was the principal reason for the smog. Extending his fascination about enzymes, he developed and patented an exhaust fume catalytic converter for treating emissions from petrol engines. This patent was granted in 1956 [17]. Despite of early instances of patent, it was not until 1973 for the widespread use of industrial aftertreatment devices. The first industrial three-way catalytic converters (TWC) were introduced in the US markets in 1973 [18]. The earliest cars that had TWC with feedback lambda sensors were from 1979.

Three way catalytic converters and oxygen storage catalysts are the main aftertreatment options for SI engines. Haren Gandhi was a doctoral student in the University of Detroit,

when the Clean Air Act was passed. This was in 1970. This act decreed that the automotive emissions be controlled stringently. Haren Gandhi was then associated with the Ford motor company and the team of emissions control. He started his research with the TWC. TWC oxidises carbon monoxide and hydrocarbons to carbon dioxide and water, and reducing nitric oxide and other oxides of nitrogen to nitrogen and water. Gandhi's role was instrumental in reduction of the precious metals used in the catalytic converters by reusing and recycling the catalysts and by process intensification.

He then, worked along with his colleagues and found that the capabilities of a TWC can be enhanced by the oxygen concentration. He invented a catalytic substance that would store oxygen during the fuel lean phase and release the stored oxygen during fuel-rich phase. The OSC had improved the performance of TWC very much. Gandhi is also credited with his works on catalytic poisoning by lead. His role in banning the use of leaded gasoline in the United States was very instrumental. Gandhi had 62 patents, all in automotive exhaust catalysis, to his credit. He was also named as Henry Ford Technical fellow, an honour that very few Ford employees had achieved. After his passing, Ford has established Dr Haren Gandhi Research and Innovation Award [19].

2.2 Working of catalytic converter

The goal of an aftertreatment system is to convert components from the engine-out gases to less harmful ones. The catalytic converter is a honey-comb monolith. Figure 2.1 a picture of a catalytic converter.The monolith is porous and has numerous parallel channels. Monoliths are created from porous material such as cordierite. The walls of the channels are "washcoated" with precious metal dispersed in the highly porous substrate. The washcoat offers a large active surface for the catalytic reactions. The thickness of the washcoat varies from 10 μm to 150 μm [16]. The monolith is usually held in a metallic cage, that serves to protect it from fracture .

The gases from engine travel through the channels in laminar flow. They come into contact with the catalytic walls. The advantages of using the monolith is multifold. Firstly, it offers a large surface-volume ratio. Secondly, the pressure drop experienced by the gas flow is small. Besides these, there are other purposes that a monolith provides, for example, geometry provides "uniform flow" . In addition, the monolith can also function as sieve to trap particulates that are smaller than the channel size.

Monoliths are manufactured in various cross sections, viz., circular, square, hexagonal and so on. They also have different sizes. Cells per square inch (CPSI) is a measure of the cell density or the number of channels in the monolith. Cordierite, metal foams, alloys are some of the materials of support for the monolith. The vibrations from the engine, thermal gradients and flow surge affect the ceramic substrated monoliths.
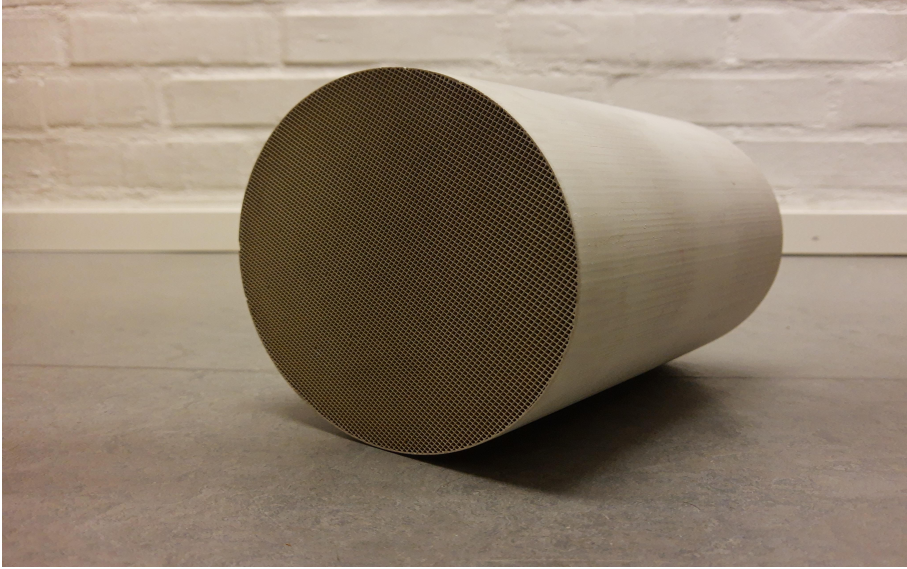
Figure 2.1: *Commercial Catalytic converter*

2.3   Transport processes in a catalytic converter

Figure 2.2 shows the different transport processes that occur in a catalytic converter. The transport processes that happen inside the monolithic catalytic converter are complex and they span different timescales. The channels provide an open structure for the flow of gases in and out of the channel. The gases from the engine that have to be treated are fed to the catalytic converter. These gases transfer momentum, mass and energy in the channels. Homogeneous reactions are activated due to virtue of temperature existing inside the channel. Heterogeneous catalytic reactions are active on the walls. The species can move axially by convection and radially by diffusion. The radial movement of species towards the wall allow the species to adsorb onto the active catalytic sites. These radicals from the engine-out species are converted to less-harmful species. The desorption and outward radial movement, again by diffusion and convection create the tail pipe emissions from the EATS. Advective transport occurs along the axial direction. The transport is diffusive along the radial direction. Temperature field inside the monolith is influenced by the heat of reactions of the homogeneous and heterogeneous chemical reactions[16].

Energy is transferred within the monolith and to the ambient. Heat is convected along the axial direction, by the gas flow through the monolithic channels. The solid walls get heated by the hot gases and by catalytic heat of reaction. The hot walls exchange heat with gases and lose heat to the ambient. The catalytic converters are usually insulated with multiple layers of insulation. The heat loss to the ambient from the walls is deterred by the insulation. Radiative heat transfer is pronounced after light-off temperatures.
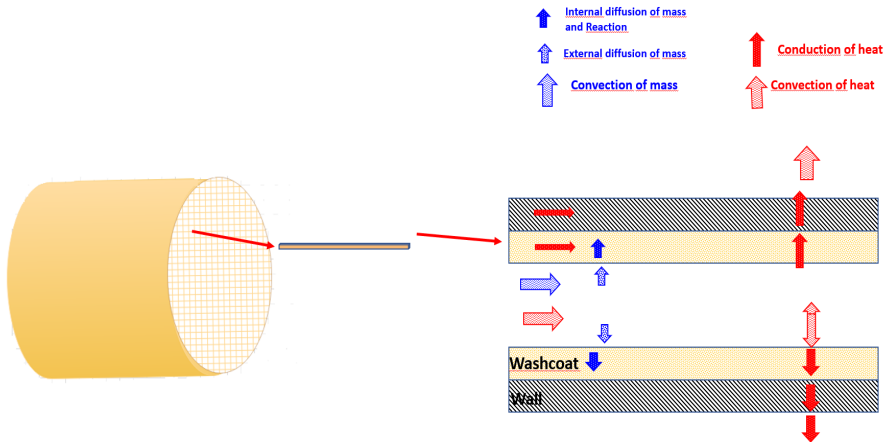
Figure 2.2: *Transport Processes in a catalytic converter.*

The performance of a catalytic converter is a function of temperature. The range of temperatures upto which the performance (conversion) of the catalyst is maximum is termed as the catalyst window. The conversion of the reactants depends on the size of the catalyst, active metal loading and the residence time of reactants in the catalyst. This residence time is expressed as Gas Hourly Space Velocity (GHSV), which has units of inverse of time (hours). Another important characteristic of the monolith is the *light-off* temperature. This is temperature at which atleast 50 % of the reactants are converted. This is also the temperature when the rate controlling regime shifts from kinetics control to mass transfer control.

2.4   Single Channel Model (SCM)

One important performance criterion is the conversion in catalytic processes. To get this information, different forms of rate expressions are used. The rate expressions are generally used in the Arrhenius form, with a pre-exponential factor and an activation energy. Inhibition term in the rate expression may include the change in catalytic activity because of ageing or catalyst poisons. Alternatively, a microkinetic model or a detailed kinetic model can be developed. In this model, the physical processes are modeled as elementary reactions with a corresponding rate. These rate expressions are usually incorporated in transport equation. Heat effect and mass transfer effects are also modeled in these expressions through transport coefficients.

A mathematical model representing convection-diffusion-reaction (CDR) processes in a monolith is developed to solve for velocity, temperature and concentration. A monolith has multiple channels. There is energy interaction between channels. A complete 3D model in the differential form is a representation of the equations of change in the monolith. To ease the computational complexity, a single channel is chosen and this representative

channel is assumed to be emulating all the channels in the monolith. This model is called the single channel model (SCM). According to this assumption, it is sufficient to solve for C, V, T for this one channel [20]. To satisfy equation of continuity, velocity has to remain constant when the flow area has constant area of cross section with constant density. Therefore, species mass balance and energy equation can give solution to C and T in the representative channel.

It is important to note that the velocity in a channel in the monolith is essentially laminar. This laminar flow produces a parabolic profile inside the monolith. The length of monolith may also introduce entrance effects and exit effects. These factors minimize the validity of SCM.

2.5 Flow distribution in catalytic converters

The flow to the catalytic converter from the engine is usually transient and has fluctuations. The catalytic converter placement introduces bends. These create a non-uniform flow to the catalytic converter. This creates a flow distribution at the inlet of the monolith. This flow distribution puts a limitation on the SCM assumption.

2.5.1 Effects of Flow maldistribution

The flow mal distribution is predominant in the inlet and exhaust manifolds in the engine and entrance and exit regions of the diffuser. Flow maldistribution is important to be given attention due to the following reasons [21]:

- Flow maldistributions leads to differences in flowrates within the catalytic converter. Usually, single channel model (SCM) is applied to model catalytic converters. The inherent assumption is that all channels in the catalytic converters behave exactly similar in terms of conversion and temperature. This assumption does not hold when there are differences in flow or when there is flow maldistribution. Differences in flowrates introduces variable residence times in the channels. This manifests as variable conversion rates in the channel.

- Some regions of the catalyst experience lower flow than the other, this leads to non-uniform utilization of catalyst.

- Flow maldistribution also leads to temperature distribution in between the channels. Some channels experience higher temperatures. The temperature distribution also affects the light-off characteristics and conversion. It also affects attrition and ageing of catalysts.

- Heat losses are common in engine and aftertreatment systems. Flow maldistribution coupled with heat losses are important, in the view that they affect the sensors signal. These signals are required to monitor the tail pipe emissions.

- Flow maldistribution also affects the functionality of the catalytic converter.

2.5.2 Factors affecting flow maldistribution

The activity of catalytic converters are dependent on temperature. The catalytic converter attains its rated performance above its light-off temperature. To ensure rapid heating of the catalyst, the monolith can be placed close to the engine (close coupled catalysts) or far away from the engine (underbody catalysts). Catalytic converters have inlet and exit cones, that are regions for mixing. The angle of the cone is an important factor. This angle is kept small to reduce flow separation. This is a limitation due to compactness in automotive design. Holmgren et al [22] have shown that the inlet cone of the converter influences flow uniformity significantly. The inlet fluctuations also affect the uniformity of flow to the monolith. Fluctuations alter the mass flow to the catalyst. In a classical monolith, there is no mass transfer between channels. To improve flow distribution inside the monolith, Periodic Open Cellular Substrates (POCS) can be considered, which allow transfer of mass between channels and hence improve flow distribution [23].

2.6 Flow uniformity

If the incoming flow to the EATS has a distribution, then an index is used to describe this distribution. The index is termed as Uniformity Index (UI). The UI is a dimensionless scalar, and is an averaged ratio that is calculated at any plane in a catalytic converter. Exit plane of the monolith and exit of the catalytic converter are usually chosen to describe the UI.

UI gives the deviation of a flow variable from the mean value of the flow variable. UI is given by the formula [24]:

$$\gamma_a = 1 - \frac{1}{2} \left(\frac{\sum\limits_{i=1}^{n} \mid \phi_i - \overline{\phi_a} \mid A_i}{\overline{\phi_a} \sum\limits_{i=1}^{n} A_i} \right) \tag{2.1}$$

where

$$\overline{\phi_a} = \frac{\sum\limits_{i=1}^{n} \phi_i A_i}{\sum\limits_{i=1}^{n} A_i} \tag{2.2}$$

where ϕ_i is the flow variable (velocity, temperature) in the face i, $\overline{\phi_a}$ is the area-weighted average of the flow variable, and A_i is the area of face i.

The range of values of UI is from 0 to 1. The flow is considered to be very uniform for values of UI closer to 1. A 20% relative deviation in the flow from the mean (term within the brackets), will give a flow uniformity index of 0.9. UI is affected by the angle

of the inlet cones of the monolith, pulsations or fluctuations in the inlet velocity, inlet conditions such as the velocity, temperature and concentration. It is noteworthy that a difference of flow variable from the average value is used in the definition. The choice of the definition of flow variable influences the value of UI. A detailed analysis is presented in Paper I. Several definitions are used by researchers to express the UI [25–27]. Since the simulations in this work are carried out in ANSYS Fluent, the definition followed in ANSYS Fluent is used in this work [24].

UI can be estimated by experimental techniques or by simulation. Measured value of the flow variable is required, techniques like hot wire anemometry can provide the velocity at a point. Thermocouples can be used to record temperature measurement. The limitation with measurements is that the probe for measurement should not interfere with the flow path or flow field. Non-destructive techniques like Particle Image Velocimetry (PIV) or Laser Induced Fluorescence (LIF) can come handy in getting the distribution at the inlet and/or exit in optically transparent rigs. UI can also be obtained through simulations. To this end, solutions to the equations of momentum, energy and species are required. The advantage with CFD is that the UI can be calculated at any plane of interest in the monolith.

2.7 Existing literature and knowledge gap

The key to near zero emissions is the prediction of conversion in the EATS. Several studies have attempted to improve the performance of the model. Earliest works with the labels of SCM can be attributed to the works by Young and Finlayson [28, 29] and Oh and Cavendish [30]. These works described 2D variations in temperature field and the solution to CDR respectively. Further improvements with modeling of the monolith were attempted, viz., effectiveness factor to include the species diffusion in the washcoat [31], oxygen storage in 1D model [32], prediction of light-off curves using detailed kinetics [33], or the use of 1D heterogeneous model with global kinetics [34], capturing mass transfer effects on a 1+1D model [35], or a model that captures the washcoat geometry effects [36]. To include heat and mass transfer effects, correlations of Nusselt number and Sherwood number have been used to relate the transport processes with the monolith wall and the interior [32, 37].

Several works have reported the steady state uniformity index analysis in catalytic converters using CFD simulations [25, 27, 38]. These works either resolved a the monolith channels individually by modeling a limited number of channels[27] or by following a porous media approach to describe the monolith [38] or by describing the pressure drop relation in a more detailed manner [39]. Studies like [39] have attempted transient simulation too. Aslanjan et al [40] have described a multichannel model that introduces variation in inlet temperatures alone in a monolith .

One major limitation with the above works is that flow distribution data is not incorporated into the SCM. In this work, an attempt is made to demonstrate that there is

significant distribution in terms of velocity, temperature and concentration in a monolith. Therefore, a multi channel model would be required to capture the conversion under difficult conditions like coldstart and RDE. This is studied by experiments measuring temperature in a muffler and by transient CFD simulations. Paper I is about describing flow distribution in the muffler using transient CFD simulations under non reactive conditions. Paper II considers the effect of inlet fluctuations and pulsations on time averaged conversion and UI using reactive CFD simulations.

3 Experiments

Experimental features and modeling methodology are described in this chapter. For further information, publications I and II can be referred to. The construction of the experiment rig along with its associated instrumentation are presented in this section.

3.1 Experimental Rig

The EATS rig used in this study is designed to capture the relevant features of an industrial EATS fitted in a vehicle, that it should have bend and/or a dead volume, that creates a recirculation zone. The experimental rig should also be operated in transient condition. The rig should also operate under cold and warm conditions. Figure 3.1 shows the experimental rig.
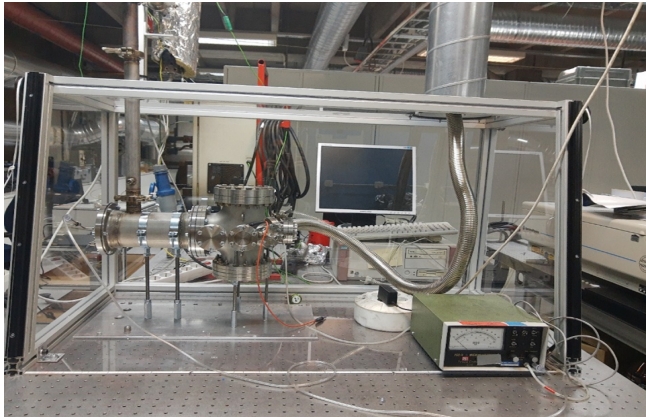
Figure 3.1: *Experimental Rig*

The experimental rig is called as "Academic Muffler". It has a vertical section and a horizontal section. The vertical section has the inlet port. The vertical section is fitted with a catalyst that acts as a flow straightener. The section is long enough so that the flow is fully developed in the vertical section. The inlet section is 3 cm in internal diameter and 50 cm long. The material of construction is stainless steel (SS310). The horizontal section is connected to the vertical section by a 90 °bend. The right side of the horizontal section houses the catalyst.

The catalyst is a diesel oxidation catalyst (DOC). This is kept insulated by layers of glass wool. The dimensions of the catalyst are 9.5 cm in diameter and 15 cm in length. This is the main catalyst. The inlet pipe is also fitted with a small catalyst, that serves to dampen the flow. This small catalyst is also wrapped inside layers of insulation.

15

The muffler is provided with ports for the passage of working fluids. The working fluids are air and nitric oxide. Air is the working fluid for flow and temperature profile visualization. Nitric oxide (NO) gas along with air will be used for species profile visualization. Air is injected from the vertical section, whereas small circular nozzles in the horizontal will be the entry port for nitric oxide. The role of nitric oxide is more of a tracer that will be illuminated via laser to get concentration profiles in the catalyst. Expanding mat is used to hold the catalyst in place and to minimize heat losses.

3.2   Associated Instrumentation

Three mass flow controllers (MFC) of capacities 1000 slpm, 200 slpm and 2 slpm (Bronkhorst) are used to regulate the flowrate of air, diluent air and nitric oxide gas respectively. The flowrates are specified at STP [1]. K-type thermocouples are inserted at the front and rear ends of the catalyst in the horizontal section to measure temperatures in the channels of the monolith. Three more thermocouples are placed on the vertical pipe for further measurements that are required for controlling the temperature and tuning the heat transfer coefficients. The fluids that are used in the experiment are heated by using a Eurotherm fitted with controllers for close control of temperatures. Positive drought is ensured for flow of gases from the muffler, by calibrating the pressure drop across the ventilation lines. The data acquisition is accomplished by in-house LabVIEW module. This also helps in running automated flow experiments. the muffler is attached to an optically active chamber for use of laser diagnostics. Gaskets and seals used in the muffler and optical chamber are chosen that they are compatible with NO gas. The experimental rig is enclosed in a ventilated hood.

The nitric oxide gas cylinders are stored in gas cabinets that can withstand high temperature for a period of 90 minutes. The gas line is secured with multiple regulators and non-return valves for safe flow of nitric oxide. Leak alarms are placed inside the hood and in the experimental area. This is because the allowable leak for NO gas is very stringent.

3.3   Calibration Experiments

Pressure drop in the horizontal section was measured by manometer by varying the flowrate at the inlet. This information is required in the porous media to specify the resistance to the flow in the monolith in the simulations.

---

[1]Standard Temperature and Pressure (STP) 273.15 K and 101.325 kPa
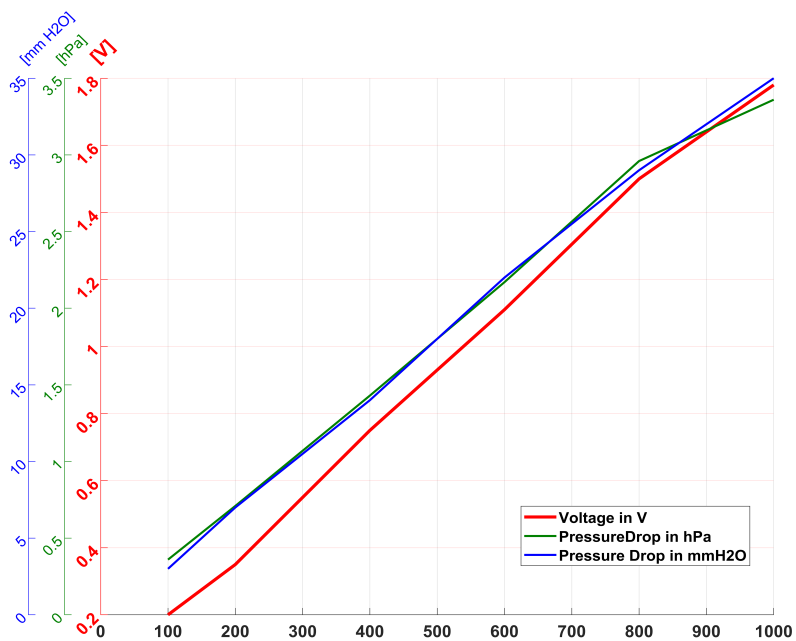
Figure 3.2: *Pressure drop Vs Flowrate Calibration*

4 Modeling

The flow maldistribution analysis requires the velocity, temperature and concentration information on a plane or surface, as the uniformity index is a ratio of area weighted average of the flow parameter to the product of average flow variable and the area of the cell. The model that is used in the CFD simulations has two sections: a non-catalytic part and a catalytic part. First, the governing equations for the non-catalytic section is described followed by the catalytic section model.

The following assumptions are made in the model development:

- The working fluid that is used in the simulation is air. The gas phase is assumed to be ideal at the operating conditions and Newtonian .

- The monolith is assumed cylindrical with circular cross section.

- The flow is a non-reactive flow and is incompressible.

- Radiation effects are insignificant at the operating conditions

- Laminar flow is enforced in the catalyst section.

- Gravity effects are not included in the model.

4.1 Flow Field

The flow field is characterized by the velocity components, temperature and species concentrations. The flow field has to satisfy the law of conservation of mass, momentum and energy. The balance equations of these variables on a control volume are a set of differential equations. The law of conservation of mass leads to the continuity equation. The momentum balance equation is obtained from the Newton's second law of motion. When this is applied to a Newtonian fluid [1], the momentum balance equation is termed as the Navier-Stokes equations.

The law of conservation of energy yields the energy equation, while the mass balance on the species gives species continuity equation. To obtain the values of the flow field at any plane, the solution of Navier-Stokes equation is to be sought for the components of velocity, the energy equation for temperature and species continuity equation for the species concentrations. These equation are collectively termed as equations of change, as they are cast in the differential form. Solution of these equations gives the spatial and temporal description of the flow field. The energy and species continuity equations may have source terms like heat loss or presence of a reaction term [41].

---

[1]A Newtonian fluid is one that obeys Newton's law of viscosity. It is given by $\tau = -\mu \frac{dv}{dy}$.

The equations of change are partial differential equations. They require appropriate initial and boundary conditions for the solution. The no-slip conditions are enforced at the wall, where velocities are zero for a stationary wall. Other specifications may include Dirichlet or Neumann or mixed boundary conditions.

4.1.1 Unsteady Reynolds Averaged Navier-Stokes equations

The velocity component is a fluctuating quantity. To solve the momentum equations for the velocity contributions at every node, the computational effort is huge as the equations are complex, non-linear and coupled. One way to reduce the computational complexity is to express the velocity as two components: a mean component ($\overline{u_i}$) and a fluctuating component (u_i'). Then, by applying Reynolds Averaging procedure, the momentum equations are only for the averaged velocity components. The time scale for averaging is so chosen that it is much larger than the frequency of fluctuations, but smaller than the time period of the mean flow. This procedure gives rise to a term $\rho \overline{u_i' u_j'}$, denoted as Reynolds Stresses. This term can then be handled appropriately by a turbulence model [42].

Time-averaged Navier Stokes equation by Reynolds Averaging procedure is termed as Unsteady Reynolds Averaged Navier-Stokes (URANS) equations, these are solved to obtain the flow field variables. The turbulence is modeled in terms of appropriate turbulence modeling [42]. The URANS formulations reduces the computational load quite significantly. The limitations of a turbulence model are wall bounded flows, turbulent fluctuations and geometries of non-circular cross section [43].

4.1.2 Turbulence Modeling

In the laminar part of flow, the shear stress is proportional to the velocity gradient. Molecular viscosity is then used as the proportionality constant. On the same lines, we can assume that the Reynolds stresses have the same form as the laminar counterpart. The apparent turbulent shear stress is proportional to the mean strain. This is the Boussinesq hypothesis [42]. The proportionality constant is the turbulent viscosity or eddy viscosity.. Computing turbulent viscosity is done by a turbulence model, in terms of turbulent kinetic energy (k) and turbulent dissipation rate (ε) or specific dissipation rate (ω). The turbulent viscosity can then be used to compute the Reynolds stresses [44].

In this work, Shear Stress Transport SST $k-\omega$ model is chosen to compute the turbulent viscosity. The advantages of SST $k-\omega$ model are: (1) it is suited to handle low Reynolds number flows (2) it can handle the viscous sub-layer (3) it can handle transition flows.

4.2 Computational Solutions - CFD

The URANS equations, energy and species continuity equations can be solved for the complete domain of interest. Owing to their non-linear and coupled nature, analytical

solutions are but, available for very simplified cases. For a realistic problem, solution methodology can be obtained numerically. Experimental observations can also provide solutions, more often, for a limited number of cases. The numerical solutions are usually termed as Computational Fluid Dynamics (CFD) solutions. A number of software, commercial or open source are available for getting CFD solutions. The original differential equations are converted to algebraic equations by discretization process [45]. The solutions are usually iterative. The advantages with CFD solutions are: they provide information about the entire flow domain of interest. The validation of these solutions can be done with experimental data and /or physical laws.

There are three different CFD approaches, depending on the methodology adopted by the solution. They are the finite difference method, finite volume approach [46] and the finite element approach [47]. In this work, finite volume approach is adopted and a commercial software ANSYS FLUENT is used for the CFD solutions.

4.3 Governing equations

The equations of continuity, momentum, energy and species concentration are presented in this section.

4.3.1 Non-catalytic section

The equations that are solved are the continuity equation, momentum balance equation for the velocity components, the energy balance equation. The equations of continuity, momentum and energy are time-averaged by Reynolds Averaging procedure and they are presented below in the differential form. The time-averaged variables are denoted with the overhead bars.

The equation of continuity in the time-averaged form is given below. The overhead bar is used to represent the variable in the time-averaged form.

$$\frac{\partial \rho}{\partial t} + \frac{\partial (\rho \bar{u}_j)}{\partial x_j} = 0 \tag{4.1}$$

Here, x and t represent spatial and temporal coordinates respectively, the fluid density is given by ρ in (kg/m^3), and $\overline{u_j}$ is the time-averaged velocity (m/s) in coordinate direction x_j .

The time-averaged momentum balance equation is

$$\rho \left(\underbrace{\frac{\partial \bar{u}_i}{\partial t}}_{\text{local acceleration}} + \underbrace{\bar{u}_j \frac{\partial \bar{u}_i}{\partial x_j}}_{\text{Convective acceleration}} \right) = \underbrace{-\frac{\partial \bar{p}}{\partial x_i}}_{\text{Pressure gradient}} + \underbrace{\frac{\partial \tau_{ij}}{\partial x_j}}_{\text{Gradient of Stress}} + \underbrace{S_i}_{\text{Sourceterm}}$$

(4.2)

where p is the pressure (Pa), S_i is a source term representing the presence of the monolith brick on the flow (kg/m·s), $and \tau_{ij}$ is the stress tensor:

$$\tau_{ij} = \underbrace{\left(\mu \frac{\partial \bar{u}_i}{\partial x_j} + \frac{\partial \bar{u}_j}{\partial x_i} \right)}_{\text{Laminar Shear Stress Contribution}} - \underbrace{\rho \overline{u_i' u_j'}}_{\text{Reynolds Stress (Turbulent Contribution)}}$$

(4.3)

μ is the dynamic viscosity of the fluid (Pa.s).

4.3.2 Turbulence Modeling

The SST $k - \omega$ model is used for turbulence closure, to estimate the Reynolds stresses. The Reynolds stresses are estimated via the turbulent viscosity. Two equations, one each for the turbulent kinetic energy k (m^2/s^2), and the specific dissipation rate ω (1/s) are needed to model turbulent viscosity [44]. The transport equation for k is

$$\frac{\partial(\rho k)}{\partial t} + \frac{\partial(\rho \bar{u}_j k)}{\partial x_j} = P - \beta^* \rho \omega k + \frac{\partial}{\partial x_j} \left[(\mu + \sigma_k \mu_t) \frac{\partial k}{\partial x_j} \right]$$

(4.4)

where P is the production limiter, β^* is the closure constant used in the model, and σ_k is the turbulent Prandtl number for the turbulent kinetic energy (k) and μ_t is the turbulent viscosity. The transport equation for ω is

$$\frac{\partial(\rho \omega)}{\partial t} + \frac{\partial(\rho \bar{u}_j \omega)}{\partial x_j} = \frac{\gamma}{\nu_t} P - \beta \rho \omega^2 + \frac{\partial}{\partial x_j} \left[(\mu + \sigma_\omega \mu_t) \frac{\partial \omega}{\partial x_j} \right] + \\ 2(1 - F_1) \frac{\rho \sigma_{\omega 2}}{\omega} \frac{\partial k}{\partial x_j} \frac{\partial \omega}{\partial x_j}$$

(4.5)

where β is a closure constant, γ is the ratio of β and β^*, ν_t is the turbulent kinematic viscosity, σ_ω is the turbulent Prandtl number for ω, $\sigma_{\omega 2}$ is also a closure constant, and F_1 is a damping function.

More specifically,

22

$$P = \tau_{ij}\frac{\partial \bar{u}_j}{\partial x_j}$$

$$\tau_{ij} = \mu_t\left(2S_{ij} - \frac{2}{3}\frac{\partial \bar{u}_k}{\partial x_k}\delta_{ij}\right) - \frac{2}{3}\rho k\delta_{ij}$$

$$S_{ij} = \frac{1}{2}\left(\frac{\partial \bar{u}_i}{\partial x_j} + \frac{\partial \bar{u}_j}{\partial x_i}\right)$$

The following formula is used to compute the turbulent viscosity:

$$\mu_t = \frac{\rho a_1 k}{max(a_1\omega, \Omega F_2)}$$

The damping functions and other constants required to compute the turbulent viscosity are obtained as shown below:

$$\phi = F_1\phi_1 + (1 - F_1)\phi_2$$

ϕ_1 and ϕ_2 are the inner constants 1 and 2.

$$F_1 = tanh(arg_1^4)$$

$$arg_1 = min\left[max\left(\frac{\sqrt{k}}{\beta * \omega d}, \frac{500\nu}{d^2\omega}\right), \frac{4\rho\sigma_{\omega 2}k}{CD_{k\omega}d^2}\right]$$

$$CD_{k\omega} = max\left(2\rho\sigma_{\omega 2}\frac{1}{\omega}\frac{\partial k}{\partial x_j}\frac{\partial \omega}{\partial x_j}, 10^{-20}\right)$$

$$F_2 = tanh(arg_2^2)$$

$$arg_2 = max\left(2\frac{\sqrt{k}}{\beta * \omega d}, \frac{500\nu}{d^2\omega}\right)$$

In the above expressions, d is the distance to the nearest wall from the field point. Ω is the vorticity magnitude and is given by

$$W_{ij} = \frac{1}{2}\left(\frac{\partial \bar{u}_i}{\partial x_j} - \frac{\partial \bar{u}_j}{\partial x_i}\right)$$

Default constants from ANSYS Fluent were used in the work. Additional description and details about the terms and functions in the SST $k - \omega$ model can be found in [44].

The time-averaged energy equation is

$$\rho C_p \left(\frac{\partial \bar{T}}{\partial t} + \bar{u}_i \frac{\partial \bar{T}}{\partial x_i} \right) = -\frac{\partial \overline{q}_i}{\partial x_i} + \bar{\Phi} \tag{4.6}$$

where the dissipation function $\bar{\Phi}$ is given by

$$\bar{\Phi} = \frac{\mu}{2} \left(\frac{\partial \bar{u}_i}{\partial x_j} + \frac{\partial u'_i}{\partial x_j} + \frac{\partial \bar{u}_j}{\partial x_i} + \frac{\partial u'_j}{\partial x_i} \right)^2$$

and

$$q_i = -\lambda \frac{\partial \bar{T}}{\partial x_i} + \rho C_p \overline{u'_i T'}.$$

The time-averaged species continuity equation that governs the spatio-temporal evolution of the reactant mass fraction $\bar{Y}$ is as follows:

$$\left(\frac{\partial \rho \bar{Y}}{\partial t} + \bar{u}_i \frac{\partial \rho \bar{Y}}{\partial x_i} \right) = -\frac{\partial \bar{J}_i}{\partial x_i} + R \tag{4.7}$$

The term $\bar{J}_i$ represents the species flux due to diffusion and R represents the source term due to chemical reaction.

The turbulent contributions to $\overline{q}_i$ and $\overline{J}_i$ are handled within the SST $k - \omega$ framework.

4.4 Model for the Catalytic Section

The monolith section is the catalytic section. The monolith is characterised by the number of channels per square inch. This can be converted into porosity. The flow in the monolith is essentially laminar. As the flow progresses from the non-catalytic section to the catalytic section, the flow changes from turbulent to laminar regime. One other important feature of the monolith is that the flow progresses in the axial direction. The radial flow is prohibited because of the presence of channel walls.

The monolith channels can be modeled individually to obtain the flow field in the monolith. This approach would be very computationally-intensive owing to the large number of channels. Another alternate approach is to use a lumped parameter approach. In this method, the monolith is approximated as a porous media. The porous media is approximated as momentum sink. The turbulence viscosity and turbulent production are set to zero.

ANSYS Fluent uses superficial velocity formulation. The porous media is modeled by a source term in the momentum equations. The flow experiences pressure drop as it passes through the monolith. This pressure loss source term is a sum of two terms: viscous term and inertial term [24]. The inertial pressure drop is proportional to the square of velocity and the viscous term is proportional to the velocity.

$$S_i = -\left(\sum_{j=1}^{3} D_{ij}\mu v_j + \sum_{j=1}^{3} C_{ij}\frac{1}{2}\rho|v|v_j \right) \tag{4.8}$$

For the inertial term, the pressure drop is given by

$$\nabla P = -\frac{\mu}{\alpha}\vec{v} \tag{4.9}$$

For the viscous term, the pressure drop is given by

$$\nabla P = -\sum_{j=1}^{3} C_{2_{ij}}\frac{1}{2}\rho|v|v_j \tag{4.10}$$

The inertial term coefficient provides a correction factor for inertial losses in the porous medium. This allows the pressure drop to be specified as a function of dynamic head. To model the flow only transmitted in the axial direction and very negligible in the radial direction, these coefficients are specified much higher in the radial direction than in the axial direction. The resistance direction and hence, the flow direction is specified through direction vectors. The physical properties of the monolith can be specified as anisotropic.

The energy transport equations in this work uses a equilibrium model. This means that the flowing fluid and the porous media are in thermal equilibrium with each other. The properties used are effective properties, that are functions of porosity of the porous media.

4.4.1 Estimation of Porous media resistances

The inertial and viscous resistances can be obtained via experiments. Experimental pressure drop is measured at various flowrates (velocities). This can be plotted as shown in figure 3.2. An empirical model can be fit to the data with the independent variable as velocity. The coefficients of the linear term and quadratic term give the values of the viscous resistance.

4.5 Description of the methodology for the non-reactive simulations

Table 4.1: Geometry Details

Parameter	Variable	Value
Diameter of Inlet section	D_{inlet}	3 cm
Length of the inlet section	l_{inlet}	60 cm
Diameter of horizontal section	D_{hor}	10 cm
Length of horizontal section	l_{hor}	25 cm
Diameter of DOC with insulation	D_{cat}	10 cm
Length of DOC (cm)	l_{cat}	15 cm

Non-reactive simulations are carried out with base geometry that emulates the academic muffler. Vertical section contains the inlet at the top and leads the flow to the horizontal section through a 90 °bend. This bend creates a significant flow distribution at the inlet of the monolith. The dimensions of the geometry of the muffler are given in Table 4.1. The horizontal section extends asymmetrically more on the right than the left, The left sections ends as a wall with no outflow. The geometry is partitioned into 700,388 hexahedral cells.

Physical properties of the materials used in the simulation are listed in Table 4.2.

Table 4.2: Material Properties

Material	Density ρ (kg/m^3)	Specific Heat Capacity C_p (J/kg $\cdot K$)	Thermal Conductivity k (W/m$\cdot K$)
Stainless Steel	8000	502.48	16.27
Cordierite	279	1050	1.8 and 0.9
Insulating Mat	200	1080	0.057
Glass Wool	100	840	0.03
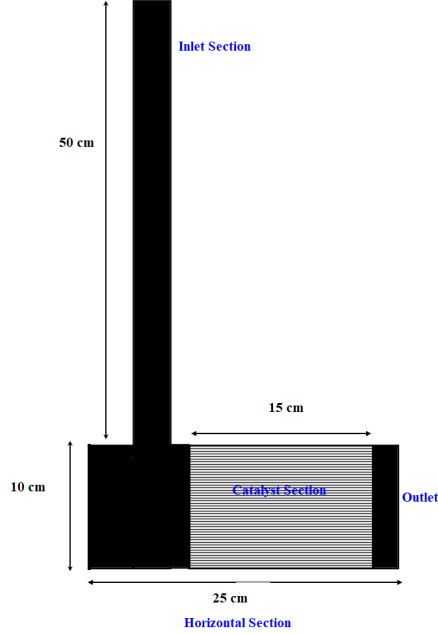
Figure 4.1: *Schematic of the academic muffler. The hatched section represents the catalytic section. The blackened region represents the non-catalytic section. The flow is from top to bottom and from left to right. The domain is half-symmetric (the illustrated cross-section represents a symmetry plane).*

4.5.1 Operating conditions and simulation cases

Two sets of transient simulations are designed to study the evolution of uniformity the development of flow field. The operating conditions are shown in Table 4.4.

4.5.2 Boundary Conditions

The inlet boundary conditions are listed in Table 4.4. A step change is introduced at $t = 0s$ and $t = 20s$ in the two cases to a velocity of 22.0135 m/s from 0 s and 11.8325 s respectively for the first and second simulation. The changes are also effected in the inlet temperature. The simulation is performed until steady state is attained in both cases. Turbulent intensity of the order of $I_{turb} = 0.16Re^{\frac{1}{8}}$ and length scale at 7 % of the hydraulic diameter are specified as inlet turbulent conditions. Temperature and velocity are passed through time dependent User Defined Function (UDF) to the simulation.

Pressure outflow is specified at the outlet boundary condition, with zero gauge pressure. The backflow turbulent intensity and viscosity ratio are set at 5 and 10 % respectively.

Table 4.3: Operating Conditions

Flow parameter	Steady state 1	Steady state 2
Volumetric Flowrate at STP (lpm)	500	948
Operating Temperature (°C)	100	93
Velocity at Operating conditions (m/s)	11.8325	22.0135
GHSV of the catalyst (h^{-1})	39189	74302
Residence time (s)	0.181	0.097

Walls are specified with no-slip boundary condition. Symmetry plane reduces the computational load.

Table 4.4: Simulation cases

Case name	0 to SS1	SS2 to SS1
Starting time (s)	0	0
Initial velocity (m/s)	0	11.8325
Initial Temperature (°C)	20	100
Step Change Time (s)	0	20
Velocity at Step Change (m/s)	22.0135	22.0135
Temperature at Step Change (°C)	93	93
Simulation Stop time (s)	35	35

4.5.3 Monolith Section

In an actual monolith, the flow is unidirectional, with no radial between channels. The flow is also laminar. The monolith is anisotropic in nature. This is realized in the simulation by specifying large resistances to flow. Viscous and/or and inertial resistances can be inputs to the porous media model for the monolith. In the current simulation, a resistance value of $2.74 \cdot 10^7 m^{-2}$ is specified as the viscous resistance for the flow direction and a resistance that is larger by three orders magnitude for the non-flow directions. The porosity of 0.72 is used this work.

To allow for heat transfer between the muffler and the ambient, a shell conduction model is used. The value of thickness of material and the heat transfer coefficient are specified. A tuned value of heat transfer coefficient that is obtained from the measured temperatures from the muffler is used in the simulations.

4.5.4 Solution Methodology

The symmetry plane is located in the middle plane of the muffler. Iterative solution strategy for handling the pressure velocity coupling by the Semi-Implicit Pressure Linked Equation (SIMPLE) method. First order upwind scheme is used for discretising the

convective terms. Second order accurate central differencing scheme is used for diffusional terms. Under relaxation factors were used for pressure, momentum, specific dissipation rate and turbulent kinetic energy. Default values were retained for the turbulent model constants and the damping functions. Convergence was ensured when the residuals dropped to atleast three orders of magnitude from the starting values. Refinement of the grid was done in the regions that showed substantial gradients. A timestep of 0.005s is chosen for the solution scheme.

4.6 Description of the methodology for the reactive simulations

Reactive simulations in a monolith are assessed to demonstrate the influence of inlet pulsations and fluctuations on the conversion of the reactants. The details of the geometry, mesh and solution methodology are discussed in this section.

4.6.1 Geometry and Mesh
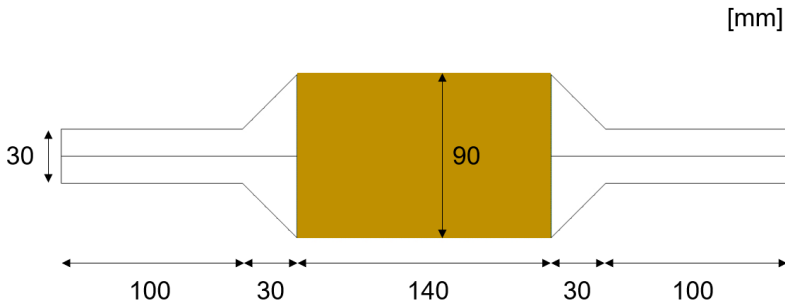
Figure 4.2: *Overview of the computational geometry used for reactive simulations. The flow goes from left to right. The domain is 2D axisymmetric and the horizontal line from the middle of the inlet represents the axis of symmetry. The dark yellow section is the monolith brick.*

A monolith with inlet and outlet cones along with connecting ducts is considered for the reactive simulations. The monolith is 90 cm in diameter and 140 mm long. This central section is connected to 45 °cones on either sides.30 mm pipes transport the reactants and products. The geometry has radial and angular symmetry. A schematic of the geometry is shown in Figure 4.2. The meshed geometry has 11093 cells, with a resolution in the range of $0.06 - 0.6$ mm at mesh-independent conditions.

4.6.2 Monolith

Porous media model is used to represent the monolith with a isotropic porosity $\varepsilon = 0.8$, with a viscous resistance specification. Thermal equilibrium is assumed between the solid

phase and gas phase. An inlet velocity of $10m/s$ and a permeability of $\alpha = 2.111 \cdot 10^{-8}$ s/m produces a pressure drop of $1000Pa$ over the monolith. The velocity in the monolith is laminar. Turbulence transport is very insignificant in the monolith.

A first order heterogeneous reaction is specified as source term through an Arrhenius type rate expression as shown below:

$$R = -\bar{Y}\rho SA \exp\left(E_A/R_{gas}T\right), \qquad (4.11)$$

where S is the specific area (wall surface available per reactor volume, m^2/m^3), is the Arrhenius frequency factor (1/s), E_A is the activation energy (J/mol), and R is the universal gas constant (J/K $\cdot$ mol). The values are $S = 4 \cdot 10^3$ m^2/m^3, $A = 2 \cdot 10^6$ s^{-1} and $E_A = 100$ kJ/mol.

The fluid properties employed are provided in Table 4.5.

Table 4.5: Material properties.

Property	Value
ρ	ideal gas law[1]
μ	Sutherland's law[2]
c_p	1006.43 J/kg,K
k	0.0454 W/m,K
D_{AB}	$2.88 \cdot 10^{-5}$ m^2/s

[1] $M_w = 28.966$ kg/kmol. [2] $\mu_0 = 1.716 \cdot 10^{-5}$ kg/m,s, $T_0 = 273.11$ K, $S = 110.56$ K.

4.7 Boundary conditions

The transient inlet boundary conditions for the various cases in the reactive simulations are specified in the Table 4.6 and graphically in Figure 4.3. The inlet pulsations are specified as a constant inlet velocity, a square inlet velocity, a sinusoidal inlet velocity and a triangular inlet velocity. The variations are specified either as a velocity inlet or as a pressure inlet. Inlet reactant concentration is also specified as mass fraction. The outlet conversion is calculated using $X = 1 - \bar{Y}_{out}/\bar{Y}_0$, where $\bar{Y}_{out}$ is the mass-weighted average of the reactant mass fraction on the system outlet.

4.7.1 Solution Methodology

The simulations are solved using a double precision based solver, on a colocated grid. The temporal derivatives are discretised by a implicit discretisation. A coupled scheme is used to handle pressure-velocity coupling . Convective terms are discretised using a third order Monotonic Upstream-centered Scheme for Conservation Laws (MUSCL) scheme. The diffusion terms are discretised using a second order central differencing scheme. Reaction

Table 4.6: The boundary condition specifications of the cases investigated in the present work. The flow inlet boundary condition is either a specified velocity or a specified pressure. The inlet temperature boundary condition is a specified temperature.

Case	Flow inlet boundary condition[1]	Temperature boundary condition[2]
Case 1	$U(t) = U_0$	$T(t) = T_0$
Case 1C	$U(t) = U_0$	$T(t) = T_0 + \Delta T \sin(2\pi t/\Delta t)$
Case 2	$U(t) = \begin{cases} U_0 + \Delta U & \text{if mod}(\text{rem}(t, \Delta t)) = 0 \\ U_0 - \Delta U & \text{else} \end{cases}$	$T(t) = T_0$
Case 2B	$P(t) = \begin{cases} P_0 + \Delta P & \text{if mod}(\text{rem}(t, \Delta t)) = 0 \\ P_0 - \Delta P & \text{else} \end{cases}$	$T(t) = T_0$
Case 3	$U(t) = U_0 + \Delta U \sin(\pi t/\Delta t)$	$T(t) = T_0$
Case 3B	$P(t) = P_0 + \Delta P \sin(\pi t/\Delta t)$	$T(t) = T_0$
Case 4	$U(t) = \begin{cases} \Delta U + U_0 t/\Delta t & \text{if mod}(\text{rem}(t, \Delta t)) = 0 \\ 3\Delta U - U_0 t/\Delta t & \text{else} \end{cases}$	$T(t) = T_0$
Case 4B	$P(t) = \begin{cases} \Delta P + P_0 t/\Delta t & \text{if mod}(\text{rem}(t, \Delta t)) = 0 \\ 3\Delta P - U_0 t/\Delta t & \text{else} \end{cases}$	$T(t) = T_0$

[1] $U_0 = 10$ m/s, $\Delta U = U_0/2$, $P_0 = 1004.3067$ Pa, $\Delta P = P_0/2$ and $\Delta t = 0.1$ s.

[2] $T_0 = 573$ K, $\Delta T = 50$ K and $\Delta t = 0.1$ s.

source terms are handled explicitly. Time step is chosen as 0.001s, to ensure that it is significantly smaller than pulsating frequencies.
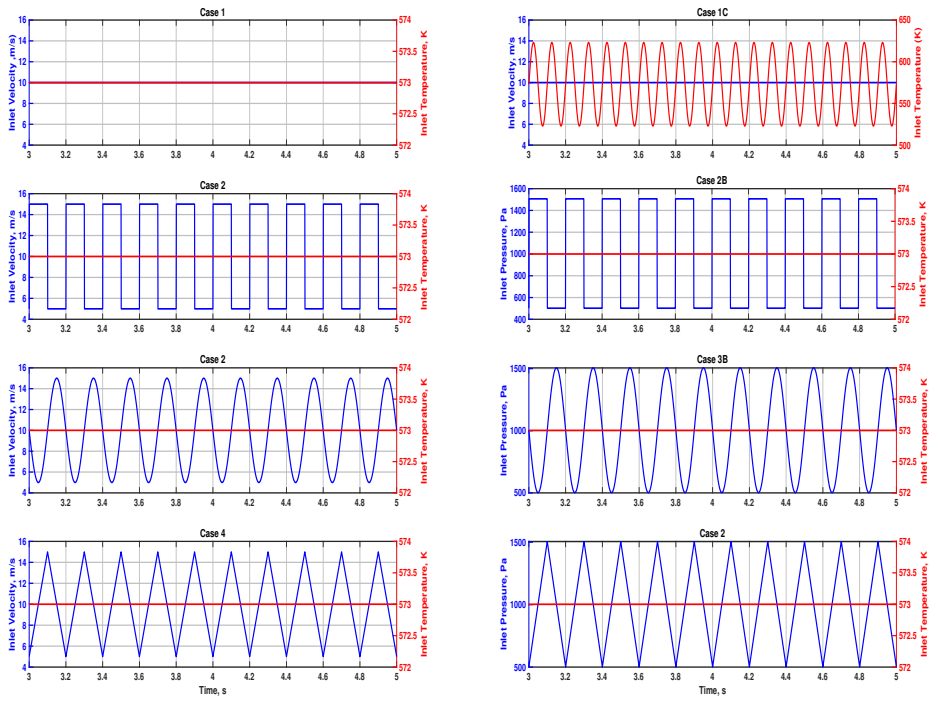
Figure 4.3: *Inlet velocities and temperatures over time as obtained in cases 1, 2, 3 and 4. The blue lines and the red lines represent velocity and temperature respectively.*

5 Results and Discussion

The main findings and implications from publications I and II are presented in this chapter as a short summary.

5.1 Summary of publication I - Transient Flow Predictions of Flow Uniformity Evolution in Geometrically Complex Exhaust Gas Aftertreatment Systems using 3D-CFD

Publication I is focused on demonstrating the limitations of the Single Channel Model. It also explains the analysis of flow non-uniformity as histograms and contours. A complex geometry with a 90 °bend and a partial dead volume is the chosen geometry. Transient step input is applied to the inlet of the geometry. The evolution of the flow field and temperature field is obtained through the solutions of Unsteady Reynolds-Averaged Navier Stokes Equations for continuity, velocity and temperature. The catalyst section is modeled using lumped porous media model. The resistances that are used in the porous model are obtained through the flow - pressure drop measurements done on the experimental rig, with hot air at various flowrates. The heat loss magnitude is also obtained by logging temperatures at several locations at the inlet and outlet of the monolith using thermocouples. These measurements gave an estimate of the heat transfer coefficient value for describing heat loss.

In the simulations, hot air at certain velocity and temperature is passed over a cold catalyst. Heat loss from the muffler to the ambient is specified using a heat transfer coefficient. One important aim of this work is to understand the interaction of the flow field with the temperature field. The fluid in the flow straightener emerges as a jet and the lower section experiences a larger flow than the upper section in the horizontal section of the muffler. The flow then squeezes into the monolith and emerges out. The heating of the muffler along with monolith competes with the heat loss from the muffler. The pressure drop experienced by the flow and the heat loss aid the evolution of uniformity. This process is captured by the contours at three locations inside the monolith and at the exit. Velocity and temperature contours show the circulation of heat inside the monolith in Figures 5.1 and 5.2. This variation is captured spatially and temporally. Figure shows the contours of velocity and temperature.

The histograms and contours of velocity and temperature demonstrate that there is hardly uniformity in terms of velocity field and temperature. The histogram distribution also depends on the inlet temperature and velocity. As a result of a widespread distribution, it will not be very intuitive to use the SCM and and one representative channel to be explaining the behaviour of all channels, that too under transient conditions is very misleading.
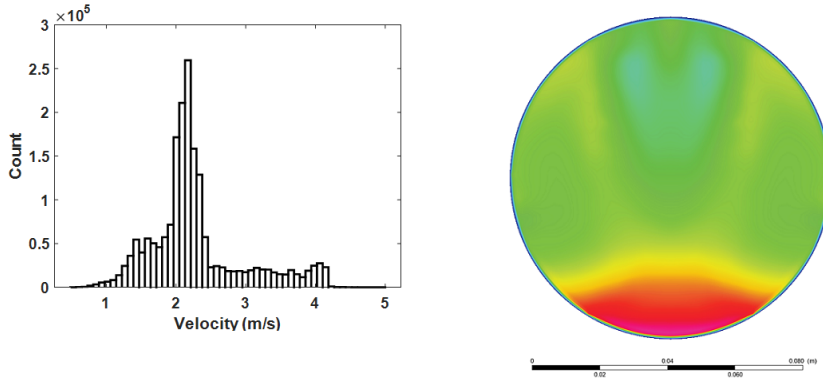
Figure 5.1: *Histogram of velocity over the monolith (left) and contour of velocity in the center plane of the monolith at the end of 35s.*
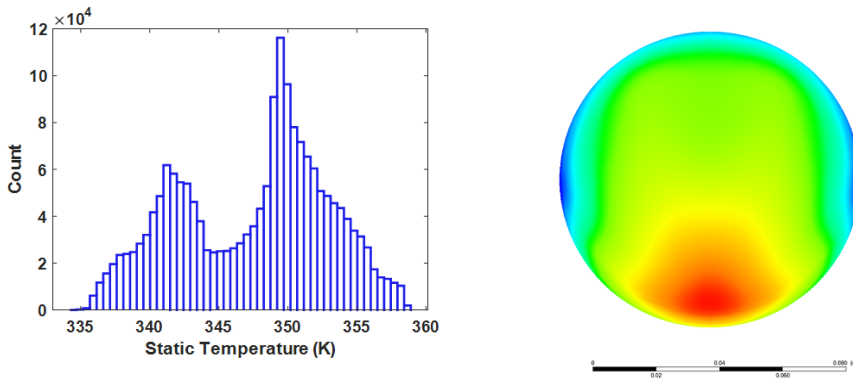
Figure 5.2: *Histogram of temperature over the monolith (left) and contour of temperature in the center plane of the monolith at the end of 35s.*

Another important outcome of this study is the implication of the value of uniformity index. In the study, a value of uniformity index was obtained for velocity and temperature. Identical values of UI does not mean identical levels of uniformity of flow field and temperature fields. A plot of UI for velocity and temperature for the two simulations cases is shown in Figure 5.3. The value of UI is decreases with increase in velocity. Lower temperature values improve uniformity. The flow parameters at the inlet increase in velocity, but decrease in temperature at t = 0. The UI value for temperature improves to a higher value whereas there is a dip in velocity UI.

Figure 5.3: *Transient variation of uniformity indices. The top panels (a) and (b) represent the temperature and velocity UI plots for the simulation* `0 to SS1` *case and the lower panels (c) and (d) represent the same for the simulation* `SS2 to SS1`. *The 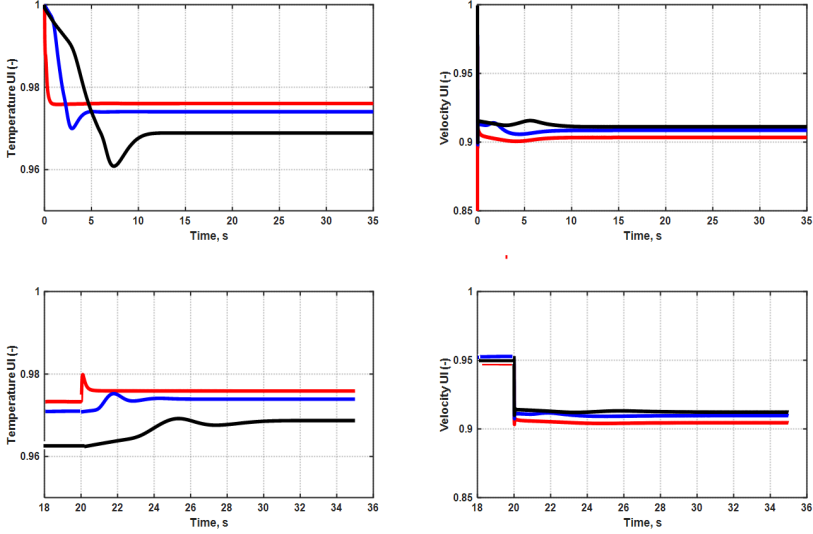location of the red line is at the entry of the catalyst, blue and black are the planes in the middle and outlet of the catalyst respectively.*

5.2 Summary of publication II - Numerical assessment of flow pulsation effects on reactant conversion in automotive monolithic reactors

Figure 5.4 shows the variation of reactant conversion as a function of time for the cases 1, 2, 3 and 4. Table 5.1 shows the time-averaged conversion, UI for all the eight cases. From the figure 5.4 and the table 5.1, the time-averaged conversion and UI are different for the various inlet velocities. There are subtle variations within a case, when the inlet flow is specified as velocity inlet or a pressure inlet. The retention time and specification method affects the conversion at the outlet. In these cases, the extremum points in velocities do not coincide with the extrema in the conversion. The dispersion mechanisms, the movement of plug within the monolith and the eventual mixing in the end cones strongly affect the outlet conversion.

Table 5.1: Time-averaged results for inlet velocity, conversion at system outlet and uniformity index inside the monolith brick. The variation intervals reported are the standard deviations. Averages and standard deviations are recorded for the last second of a 10-second run.

| Case	Velocity [m/s]	Conversion	Uniformity index	Temperature [K]
Case 1	10.0	0.538	0.9967	573.0
Case 1C	10.0 ± 0.00	0.498 ± 0.001	$0.9971 \pm 1.64 \cdot 10^{-4}$	573.0 ± 35.36
Case 2	10.0 ± 5.00	0.503 ± 0.090	$0.9966 \pm 2.79 \cdot 10^{-4}$	573.0
Case 2B	9.60 ± 4.52	0.519 ± 0.085	$0.9966 \pm 2.45 \cdot 10^{-4}$	573.0
Case 3	10.0 ± 3.54	0.514 ± 0.073	$0.9967 \pm 8.71 \cdot 10^{-5}$	573.0
Case 3B	9.66 ± 3.25	0.528 ± 0.069	$0.9967 \pm 8.83 \cdot 10^{-5}$	573.0
Case 4	10.0 ± 2.89	0.522 ± 0.060	$0.9967 \pm 6.19 \cdot 10^{-5}$	573.0
Case 4B	9.68 ± 2.66	0.535 ± 0.056	$0.9967 \pm 6.41 \cdot 10^{-5}$	573.0
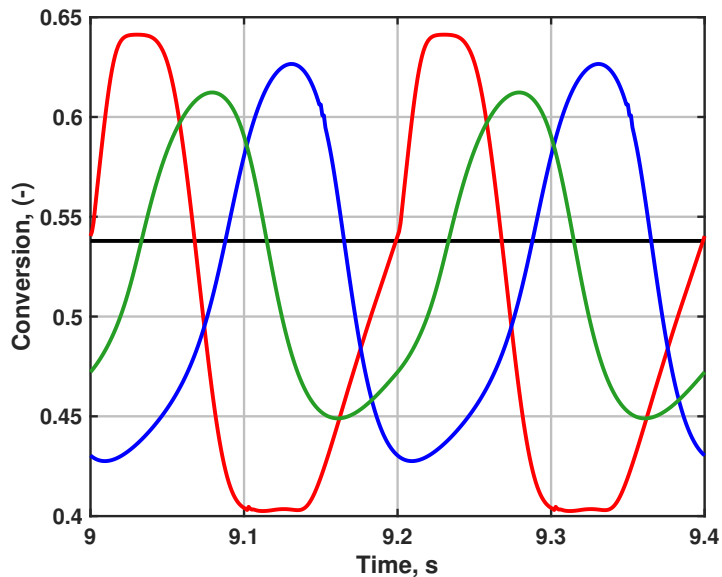
Figure 5.4: *Conversion of Reactant at the system outlet over time as obtained in cases 1 (black), 2 (red), 3 (blue) and 4 (green).*
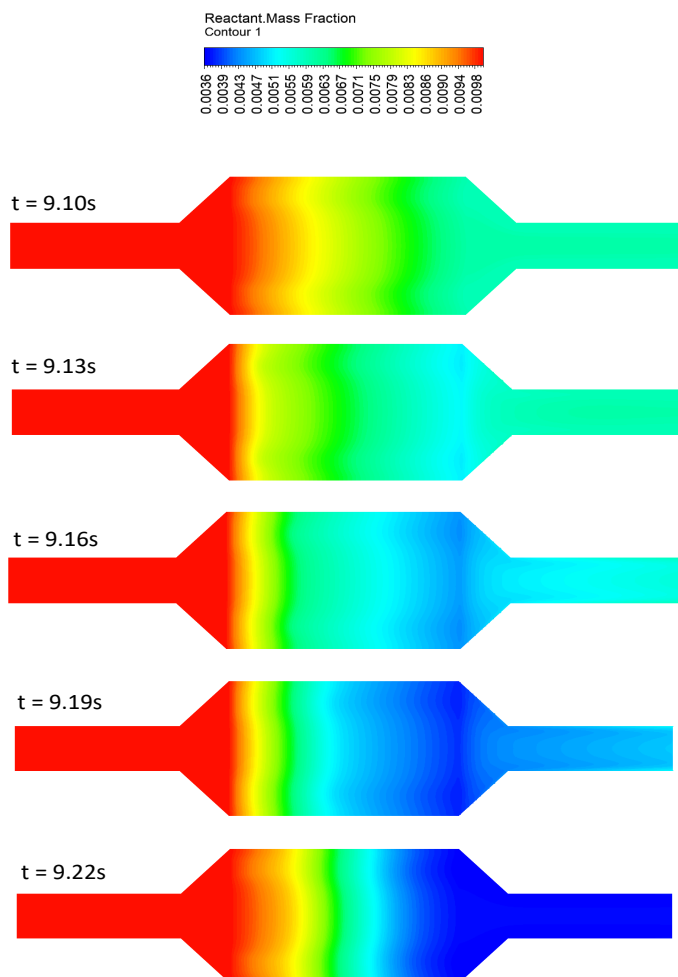
Figure 5.5: *Five snapshots of the reactant mass fraction fields for case 2 (at $t = 9.10$ s, $t = 9.13$ s, $t = 9.16$ s, $t = 9.19$ s, and $t = 9.22$ s).*

Figure 5.5 shows the movement of the reactant plug in the axial flow direction at various times as contours for the case where the inlet velocity is varying sinusoidally (Case 2).The inlet velocity decreases from 10 m/s to 5 m/s at $t = 9.10$ s and increases to 10 m/s again at $t = 9.20$ s. The existence of a low-mass-fraction region emerging from the end of the monolithic reactor is clearly visible at times $t = 9.13 - 9.19$ s, indicating that the reactant mass fraction is not monotonically decreasing along the streamwise direction when the inlet velocity is fluctuating. The times at which low reactant concentration stream emerges is between the times 9.13 to 9.19s. The other times show somewhat higher reactant concentrations. The flushing rate of the reactants is influenced by the inlet velocity.
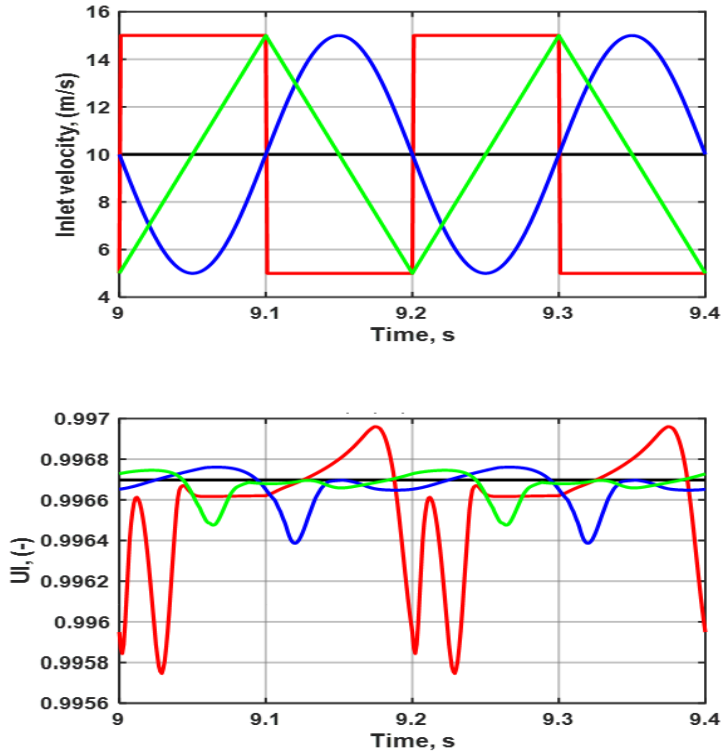
Figure 5.6: *Inlet velocity (upper panel) and Uniformity index of reactant field half-way through the monolith brick (lower panel) over time as obtained in cases 1 (black), 2 (red), 3 (blue) and 4 (green).*

Figure 5.6 shows the temporal variation of uniformity index based on reactant concentration for the simulation cases 1, 2, 3 and 4, along with the inlet velocity variation over time from 9 to 9.4s. The local variation of uniformity indices strong variation depending on the specification of inlet velocity. The UI remains constant with time, only in the case of a constant inlet velocity. All other time dependent inlet velocities show strong variation of UI. Lower velocities yield high UI and better uniformity in reactant concentration. It is also interesting to note that the peaks and valleys in the UI are out of phase with the inlet velocity. The variation in UI is strongest for pulse inlet velocity specification than the other time varying velocities. The dispersion mechanisms influence the UI and conversion in a non-trivial way, that are very distinct functions of the time dependent inlet velocities.

6 Conclusion and Future Work

6.1 Conclusion

In the Paper I, a procedure was developed to understand and analyse the flow distribution in the academic muffler, using transient non-reactive simulations.To this end, a geometry with bend and a partial dead volume is chosen to study the flow profiles in the academic muffler. Two different transients were used, to understand the evolution of the uniformity index when the system moves from steady state to another steady state. Histograms and contours were used to demonstrate the non-uniform distribution of temperature and velocity in both the simulations. Pathlines also demonstrated that the few fluid streams had travelled longer paths than some of the other fluid streams in the muffler. Another interesting result was that the value of temperature uniformity index was dependent on the definition of temperature that was used as the flow variable. Scaled temperature values with different scaling was used to evaluate temperature uniformity index. A value of 0.95 for uniformity index in temperature and velocity do not mean the same level of distribution of velocity and temperature. The temperature field evolution is slower than the velocity field because of the larger thermal mass.The temperature field influences the velocity field through the change in fluid properties. The main outcome of the study is the validity of single channel model in the presence of flow maldistribution, as the flow in such devices under transient and even steady state conditions are very complex. This study can be used to build reduced order 3D models.

The conversion in EATS is influenced by the fluctuations and pulsations in the flow to the inlet of EATS. This is the focus of Paper II. A simple reactor geometry with a catalyst is used in this study. The geometry gas cones at the inlet and outlet, these create environments for mixing. Transient reactive simulations are performed with four different inlet velocities, namely, constant, pulse, sinusoidal and triangular ramp forcing functions. It was found that the time-averaged conversions and uniformity indices are dependent on the specifications of the inlet velocity. In a reactive case, the pulsations influences the retention time in the catalyst. The retention time distribution is influenced by flow distribution in the EATS. The mixed cup conversion is found to be a function of the inlet pulsations. The nature of the transient inlet velocities affect the dispersion of the gases in the catalyst. Fluctuations in temperature also affect the reaction rates. Reaction rate is non-linearly dependent on temperature. This dependence is altered by the fluctuations in the transient inlet conditions. When the inlet velocity is specified as a pressure value, flow discontinuity propagation is minimized. The mixing in the cones is also influenced by the fluctuations.

6.2 Future Work

The current work is focused on understanding flow distribution in EATS. An experimental rig was assembled to analyse flow distribution. The analyses were further augmented

well by CFD simulations. More research is required to include the flow maldistribution information to the reactor models of EATS.

To improve the predictive capabilities of a reactor model for the catalytic converter, multichannel models are preferred over single channel models. Their use is limited owing to the large computational efforts in obtaining the solution. The following methods are being considered to include the flow distribution information in modeling:

1. A multichannel model can be developed by combining many single channel models. The single channel model give conversion of the reactant with velocity, temperature and initial concentration as input. From the 3D transient CFD results, a few channel positions can be chosen with the profiles of velocity, temperature and concentration. These channels can then become single channels that are the representative channels. The conversion of the full monolith can then be based on weighted average of or time-averaged values. The weighting scheme can be implemented using D-optimal design.

2. Alternative to this procedure, a single channel represented by the coordinates in the entry plane of the monolith can be chosen. The position of this channel can be dynamically changed based on the flow distribution information. A group of channels can also be chosen based on a moving average that depends on the flow distribution as indicated by velocity and temperature histograms or contours.

3. The inlet fluctuations have a great role in flow distribution in the catalyst. Flow induced vibrations from the engine-out emissions are turbulent in nature. These have to be characterized and included in the flow maldistribution data that will provide the conversion at the exit of the catalyst. Detached Eddy Simulations (DES) can be used to understand the role of inlet fluctuations on the flow uniformity. One important consideration is the size of the meshes that will be comparable to scales of fluctuations. The main limitation of LES studies is the time required for the simulations, and this is dependent on the mesh size. A reasonable starting guess can be taken from corresponding URANS simulations. If the inlet fluctuations are completely characterized, single channel model predictions can become very precise and realistic.

To validate the simulation results, measured flow field data is required. In the current study, experimental measurements (temperature) are generated by thermocouples. In addition to thermal data, velocity and concentration data are required. The velocity measurements can be obtained by Prandtl tube measurements or through hot wire anemometry. Laser measurements can be used to get velocity and concentration data. For example, Particle Image Velocimetry (PIV) technique can be applied to the acquire the velocity information. NO-LIF can be used to visualize the species concentration field. LIF technique can also fetch measurements of temperature too. Using Laser techniques, the flow information at the inlet of monolith can be obtained. The inlet flow distribution dictates the flow maldistribution and the stabilization of the flow field.

The experimental setup has provision for injecting NO gas at different points on the radial plane. The NO injections and the concentration profiles at the inlet and exit planes will provide information about flow distribution in reactive systems. This information will be helpful for improved performance of SCR systems and optimise the performance of ASC.

7 Contribution to the field

This main contribution of this work can be summarized as:

7.1 Publication I

"Transient Predictions of Flow Uniformity Evolution in Geometrically Complex Exhaust Gas Aftertreatment Systems using 3D-CFD"

The main contributions of this work is the demonstration of the limitations of SCM via histogram representation of velocity and temperature. This work is one of the fewer works that addresses flow distribution under transient and non-reactive conditions. The role of thermal mass and pressure drop in the flow uniformity evolution are also studied. This analysis is a potential way to develop reduced order 1D+ models. I performed all the simulations and wrote the first draft of the paper. I also participated in the analysis and evaluation of the results.

7.2 Publication II

"Numerical assessment of flow pulsation effects on reactant conversion in automotive monolithic reactors"

The influence of pulsations and fluctuations on the time-averaged conversion and time-averaged uniformity index are studied. This study showed that even with the same time-averaged inlet velocity, there are stark differences in the time-averaged outlet conversion. I performed all the simulations and prepared the results for the draft. I together with my advisors, evaluated the results and analysed them.

Bibliography

[1] *Share of transport greenhouse gas emissions.* URL: https://www.eea.europa.eu/data-and-maps/indicators/transport-emissions-of-greenhouse-gases/transport-emissions-of-greenhouse-gases-12.

[2] John B Heywood. *Internal combustion engine fundamentals.* McGraw-Hill Education, 2018.

[3] John Cooper. *PM emissions from Exhaust in EU since 2000.* URL: https://www.fuelseurope.eu/wp-content/uploads/FuelsEurope-Statistical-Report-2019-2.pdf.

[4] Jan Kašpar, Paolo Fornasiero, and Neal Hickey. "Automotive catalytic converters: current status and some perspectives". In: *Catalysis today* 77.4 (2003), pp. 419–449.

[5] Ronald M Heck, Robert J Farrauto, and Suresh T Gulati. *Catalytic air pollution control: commercial technology.* John Wiley & Sons, 2016.

[6] *Emission Control Technologies.* URL: https://dieselnet.com/tech/engine_emission-control.php.

[7] İbrahim Aslan Reşitoğlu, Kemal Altinişik, and Ali Keskin. "The pollutant emissions from diesel-engine vehicles and exhaust aftertreatment systems". In: *Clean Technologies and Environmental Policy* 17.1 (2015), pp. 15–27.

[8] Ioannis Manisalidis, Elisavet Stavropoulou, Agathangelos Stavropoulos, and Eugenia Bezirtzoglou. "Environmental and health impacts of air pollution: a review". In: *Frontiers in public health* 8 (2020), p. 14.

[9] William F Ganong. "Review of medical physiology". In: *Dynamics of blood and lymph flow* 30 (1995), pp. 525–541.

[10] Karuna Singh and Dhananjay Tripathi. "Particulate Matter and Human Health". In: *Environmental Health.* Ed. by Takemi Otsuki. Rijeka: IntechOpen, 2021. DOI: 10.5772/intechopen.100550. URL: https://doi.org/10.5772/intechopen.100550.

[11] John Cooper. *Emission Legislations from 2012 - 2025 and Phase-In Timing in different countries.* URL: https://www.continental-automotive.com/getattachment/8f2dedad-b510-4672-a005-3156f77d1f85/EMISSIONBOOKLET_2019.pdf.

[12] *History of CARB.* URL: https://ww2.arb.ca.gov/about/history.

[13] S. C. Davis and R. G. Boundy. *Transportation Energy Data Book*. English. Oak Ridge National Laboratory, Aug. 2019.

[14] Jerzy Merkisz, Piotr Bielaczyc, Jacek Pielecha, and Joseph Woodburn. *RDE testing of passenger cars: The effect of the cold start on the emissions results*. Tech. rep. SAE Technical Paper, 2019.

[15] *EU: Cars and Light Trucks: RDE Testing*. last accessed on 2022-04-29. URL: https://dieselnet.com/standards/eu/ld_rde.php.

[16] Robert E Hayes and Stan T Kolaczkowski. *Introduction to catalytic combustion*. Routledge, 2021.

[17] *Catalytic converter for exhaust gases*. last accessed on 2022-05-16. URL: https://patents.google.com/patent/US2674521A/en.

[18] I. Chorkendorff. *Concepts of Modern Catalysis and Kinetics*. Wiley-VCH, 2003. ISBN: 3527305742. URL: https://www.xarg.org/ref/a/3527305742/.

[19] *Haren Gandhi*. last accessed on 2022-05-16. URL: https://www.invent.org/inductees/haren-gandhi.

[20] Zeynep Ilsen Önsan and Ahmet Kerim Avci. *Multiphase catalytic reactors: Theory, design, manufacturing, and applications*. John Wiley & Sons, 2016.

[21] Matthias Hettel, Eric Daymo, Tobias Schmidt, and Olaf Deutschmann. "CFD-Modeling of fluid domains with embedded monoliths with emphasis on automotive converters". In: *Chemical Engineering and Processing-Process Intensification* 147 (2020), p. 107728.

[22] A. Holmgren and B. Andersson. "Mass transfer in monolith catalysts–CO oxidation experiments and simulations". In: *Chemical Engineering Science* 53.13 (1998), pp. 2285 –2298. ISSN: 0009-2509. DOI: https://doi.org/10.1016/S0009-2509(98)00080-3. URL: http://www.sciencedirect.com/science/article/pii/S0009250998000803.

[23] Leonardo Giani, Gianpiero Groppi, and Enrico Tronconi. "Mass-transfer characterization of metallic foams as supports for structured catalysts". In: *Industrial & engineering chemistry research* 44.14 (2005), pp. 4993–5002.

[24] ANSYS FLUENT. *R2021 Theory Guide-1.2 Continuity and Momentum Equations*. 2021.

[25] Anna Holmgren, Thomas Grönstedt, and Bengt Andersson. "Improved flow distribution in automotive monolithic converters". In: *Reaction Kinetics and Catalysis Letters* 60.2 (1997), pp. 363–371.

[26] Achuth Munnannur, Christopher M Cremeens, and Z Gerald Liu. "Development of Flow Uniformity Indices for Performance Evaluation of Aftertreatment Systems". In: *SAE International Journal of Engines* 4.1 (2011), pp. 1545–1555.

[27] Gaurav Agrawal, Niket S Kaisare, S Pushpavanam, and Karthik Ramanathan. "Modeling the effect of flow mal-distribution on the performance of a catalytic converter". In: *Chemical engineering science* 71 (2012), pp. 310–320.

[28] Larry C Young and Bruce A Finlayson. "Mathematical models of the monolith catalytic converter: Part I. Development of model and application of orthogonal collocation". In: *AIChE Journal* 22.2 (1976), pp. 331–343.

[29] Larry C Young and Bruce A Finlayson. "Mathematical models of the monolith catalytic converter: Part II. Application to automobile exhaust". In: *AIChE Journal* 22.2 (1976), pp. 343–353.

[30] Se H Oh and James C Cavendish. "Transients of monolithic catalytic converters. Response to step changes in feedstream temperature as related to controlling automobile emissions". In: *Industrial & Engineering Chemistry Product Research and Development* 21.1 (1982), pp. 29–37.

[31] H Santos and M Costa. "Modelling transport phenomena and chemical reactions in automotive three-way catalytic converters". In: *Chemical Engineering Journal* 148.1 (2009), pp. 173–183.

[32] S Siemund, JP Leclerc, D Schweich, M Prigent, and F Castagna. "Three-way monolithic converter: simulations versus experiments". In: *Chemical Engineering Science* 51.15 (1996), pp. 3709–3720.

[33] JHBJ Hoebink, RA Van Gemert, JAA Van Den Tillaart, and GB Marin. "Competing reactions in three-way catalytic converters: modelling of the NOx conversion maximum in the light-off curves under net oxidising conditions". In: *Chemical Engineering Science* 55.9 (2000), pp. 1573–1581.

[34] R Holder, M Bollig, DR Anderson, and JK Hochmuth. "A discussion on transport phenomena and three-way kinetics of monolithic converters". In: *Chemical engineering science* 61.24 (2006), pp. 8010–8027.

[35] Björn Lundberg, Jonas Sjoblom, Åsa Johansson, Björn Westerberg, and Derek Creaser. "Parameter estimation of a DOC from engine rig experiments with a discretized catalyst washcoat model". In: *SAE International Journal of Engines* 7.2 (2014), pp. 1093–1112.

[36] M Walander, J Sjöblom, D Creaser, B Agri, N Löfgren, S Tamm, and J Edvardsson. "Modelling of Mass Transfer Resistances in Non-uniformly Washcoated Monolith Reactors". In: *Emission Control Science and Technology* 7.2 (2021), pp. 153–162.

[37] Nikunj Gupta and Vemuri Balakotaiah. "Heat and mass transfer coefficients in catalytic monoliths". In: *Chemical Engineering Science* 56.16 (2001), pp. 4771–4786.

[38] Sruti Dammalapati, Preeti Aghalayam, and Niket Kaisare. "Modeling the Effects of the Inlet Manifold Design on the Performance of a Diesel Oxidation Catalytic

Converter". In: *Industrial & Engineering Chemistry Research* 60.10 (2021), pp. 3860–3870.

[39]   VK Chakravarthy, JC Conklin, CS Daw, and EF D'Azevedo. "Multi-dimensional simulations of cold-start transients in a catalytic converter under steady inflow conditions". In: *Applied Catalysis A: General* 241.1-2 (2003), pp. 289–306.

[40]   Jana Aslanjan, Christian Klauer, Cathleen Perlman, Vivien Günther, and Fabian Mauss. *Simulation of a three-way catalyst using transient single and multi-channel models*. Tech. rep. SAE Technical Paper, 2017.

[41]   Frank M White and Joseph Majdalani. *Viscous fluid flow*. Vol. 3. McGraw-Hill New York, 2006.

[42]   David C Wilcox et al. *Turbulence modeling for CFD*. Vol. 2. DCW industries La Canada, CA, 1998.

[43]   Charles G Speziale. "On turbulent secondary flows in pipes of noncircular cross-section". In: *International Journal of Engineering Science* 20.7 (1982), pp. 863–872.

[44]   Florian R Menter. "Two-equation eddy-viscosity turbulence models for engineering applications". In: *AIAA journal* 32.8 (1994), pp. 1598–1605.

[45]   Suhas V Patankar. *Numerical heat transfer and fluid flow*. CRC press, 2018.

[46]   Henk Kaarle Versteeg and Weeratunge Malalasekera. *An introduction to computational fluid dynamics: the finite volume method*. Pearson education, 2007.

[47]   JN Reddy. *An introduction to the finite element method*. Vol. 1221. McGraw-Hill New York, 2004.